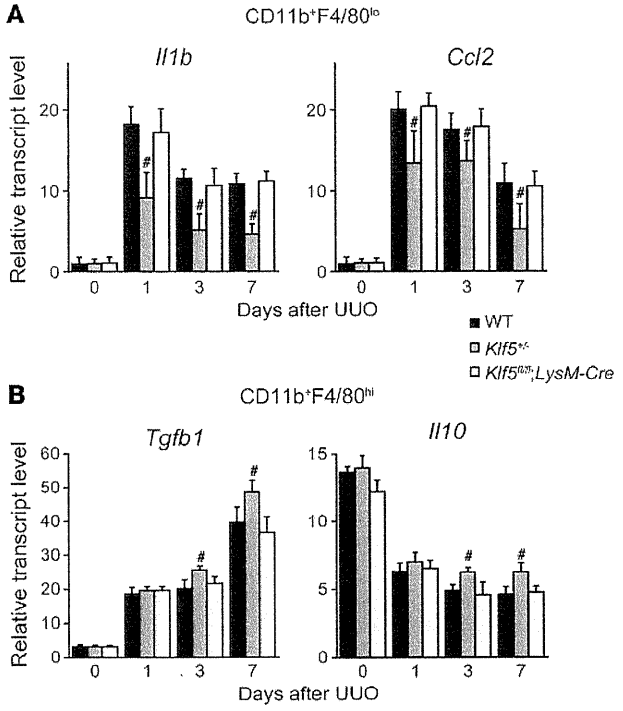

Figure 7
Effects of global and macrophage-specific *Klf5* deletion on macrophage cytokine gene expression. Expression of cytokine genes in CD11b$^+$F4/80^{lo} (**A**) and CD11b$^+$F4/80^{hi} (**B**) cells isolated from kidneys of wild-type, *Klf5*$^{+/-}$, and *Klf5*$^{fl/fl}$;*LysM-Cre* mice at indicated days after UUO. Expression levels were normalized to those of 18s rRNA and then further normalized to the levels in cells in wild-type kidney under basal conditions. $n = 3$. $^{\#}P < 0.05$ versus cells of wild-type mice at the same time point.

isolation (Supplemental Figure 8, B and C). We observed much higher frequencies of apoptosis among RTECs and mIMCD-3 cells in medium conditioned by CD11b$^+$F4/80^{lo} cells than among those in medium conditioned by CD11b$^+$F4/80^{hi} macrophages (Figure 5B). In fact, the CD11b$^+$F4/80^{hi}-conditioned medium induced apoptosis in very few cells. Moreover, the proapoptotic effect of CD11b$^+$F4/80^{lo}-conditioned medium was significantly suppressed by an anti-IL-1β neutralizing antibody. In line with these in vitro observations, inhibition of IL-1 receptor signaling by IL-1 receptor antagonist (IL-1RA) suppressed renal injury and renal cell apoptosis in UUO (Figure 5C and Supplemental Figure 9). The CD11b$^+$F4/80^{hi}-conditioned medium induced expression of *Fn1* and *Acta2*, encoding fibronectin 1 and α-SMA, in C3H10T1/2 mouse embryonic fibroblasts, which is indicative of the cells' activation into myofibroblasts, and this myofibroblastic differentiation was significantly suppressed by an anti-TGF-β neutralizing antibody (Figure 5D). These results demonstrate that CD11b$^+$F4/80^{lo} monocytes/macrophages induce renal epithelial cell injury via inflammatory cytokines, including IL-1β, whereas CD11b$^+$F4/80^{hi} M2-type macrophages appear to promote fibrosis by inducing myofibroblastic differentiation, at least in part, via TGF-β.

KLF5 controls expression of S100A8 and S100A9, which induce migration and M1 activation in macrophages. The results summarized so far suggest that renal KLF5 is involved in the accumulation of CD11b$^+$F4/80^{lo} monocytes/macrophages in the kidney. To test this possibility directly, we cultured mIMCD-3 cells infected with KLF5-expressing (Ad-*KLF5*), β-galactosidase–expressing (Ad-*LacZ*), or empty (Ad-empty) adenoviral vector in the bottom wells of Boyden chambers, and cultured RAW264.7 macrophages in the upper inserts (Figure 6A). The mIMCD-3 cells overexpressing KLF5 induced migration of significantly larger numbers of RAW264.7 cells than the cells infected with Ad-*LacZ* or empty adenovirus. This suggests that KLF5 controls production of chemoattractants. Similarly, overexpression of KLF5 in mIMCD-3 cells promoted migration of BM-derived macrophages (BMDMs) (Supplemental Figure 10A). The BMDMs had been treated with either IFN-γ/LPS or IL-4 to induce M1 or M2 activation, respectively (35), and KLF5 overexpression in mIMCD-3 cells induced migration of more M1-activated BMDMs than M2-activated BMDMs.

We then sought the downstream KLF5 effector molecules mediating the observed macrophage migration. We identified potential KLF5 target genes by combining microarray analysis with ChIP followed by high-speed sequencing (ChIP-seq) of KLF5 binding sites. We first identified genes whose expression was upregulated by Ad-*KLF5* in mIMCD-3 cells (Supplemental Table 3) and then narrowed the range of candidate genes on the basis of whether the ChIP-seq reads were in the proximity of each gene locus. Two of the candidate KLF5 target genes were *S100a8* and *S100a9*. These genes encode the secretory proteins S100A8 and S100A9, which have been shown to induce leukocyte migration (36, 37). Quantitative real-time PCR and Western blot analyses confirmed upregulation of *S100a8* and *S100a9* expression in mIMCD-3 cells infected with Ad-*KLF5* (Figure 6, B and C).

When we then tested whether S100A8 or S100A9 was capable of recruiting macrophages to kidneys, we found that recombinant S100A8 or S100A9 increased migration of RAW264.7 cells and BMDMs in Boyden chambers (Figure 6D and Supplemental Figure 10B) and that knocking down *S100a8* and/or *S100a9* significantly reduced RAW264.7 and BMDM migration induced by overexpression of KLF5 in mIMCD-3 cells (Figure 6E and Supplemental Figure 10, C and D). Both S100A8 and S100A9 more efficiently induced migration of M1-activated BMDMs than M2-activated BMDMs (Supplemental Figure 10B). Thus, S100A8 and S100A9 appear to be important chemoattractants controlled by KLF5.

In addition to the suppressed accumulation of CD11b$^+$F4/80^{lo} cells in *Klf5*$^{+/-}$ kidneys after UUO (Figure 4B), the CD11b$^+$F4/80^{lo} cells present expressed lower levels of *Il1b* and *Ccl2* than wild-type cells (Figure 7A). By contrast, expression of *Il10* and *Tgfb1* in CD11b$^+$F4/80^{hi} M2-type macrophages was increased in *Klf5*$^{+/-}$ kidneys (Figure 7B). Lin et al. recently demonstrated that circulating CD11b$^+$Ly-6C$^+$ monocytes differentiate into both M1- and M2-type macrophages in UUO kidneys (11), suggesting that the renal microenvironment plays an important role in the differential activation of macrophages. Taking this in consideration, our results suggest that *Klf5* haploinsufficiency may render the renal microenvironment relatively suppressive for M1-type activation but more permissive for M2-type activation. We therefore hypothesized that S100A8 and S100A9 might also mediate M1-type activation in UUO kidneys. To test this idea, we treated BMDMs with S100A8 and S100A9 (Figure 8A). We found they induced expression of the M1 markers *Il1b* and *Tnfa*, while the M2 markers *Arg1* and *Mrc1* (CD206) were unaffected, indicating that S100A8/A9 can induce M1-type activation of BMDMs.

S100A8 and S100A9 mediate accumulation and activation of macrophages in kidneys in vivo. To determine whether S100A8 and S100A9 also induce macrophage accumulation in kidneys in vivo, we directly injected recombinant S100A8 and S100A9 into the kidneys of mice, where they clearly induced accumulation of CD11b$^+$F4/80^{lo}

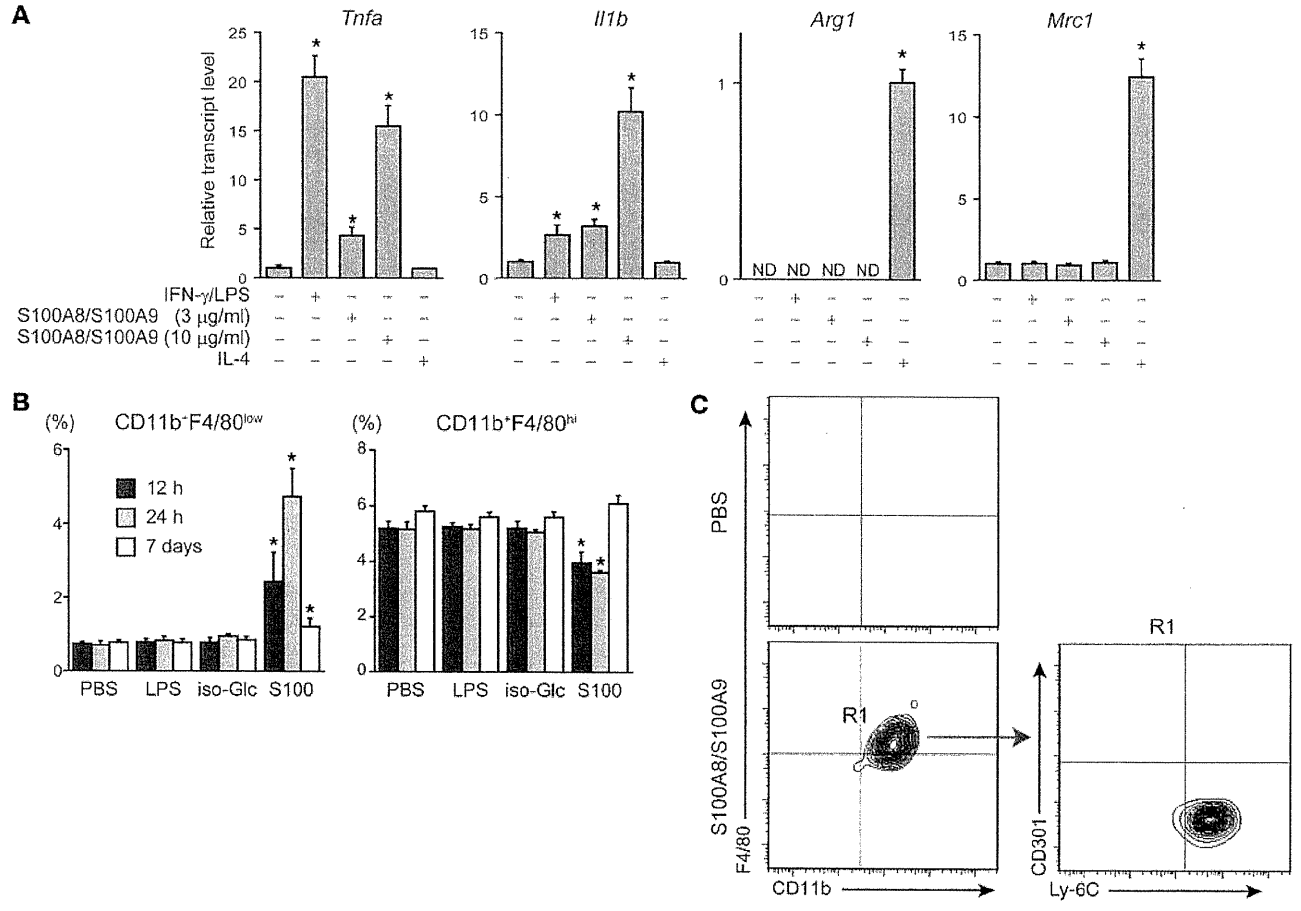

Figure 8

S100A8 and S100A9 induce M1-type activation and accumulation of CD11b+F4/80lo cells. (**A**) Effects of S100A8/A9 on M1 or M2 activation of BMDMs. Unstimulated BMDMs were treated with IFN-γ plus LPS, S100A8 plus S100A9 (3 and 10 μg/ml of each), or IL-4 for 24 hours, and expression of M1 and M2 markers was analyzed. Expression levels were normalized to those of 18s rRNA and then further normalized to the levels in BMDMs without stimulation, except *Arg1*. $^*P < 0.05$ versus untreated control. $n = 3$. (**B**) Effect of renal injection of recombinant S100A8 and S100A9 on macrophage accumulation. A solution of recombinant S100A8 and S100A9 (S100; 25 μg of each protein) was injected directly into the right kidney. The same amount of vehicle PBS, PBS containing LPS at a concentration (9.2 pg/ml) matched to that in the S100A8/A9 solution (LPS), or PBS whose osmolarity was matched to that of the S100 solution using glucose (iso-Glc) was injected into kidneys as control. CD11b+F4/80lo and CD11b+F4/80hi fractions among total live cells were determined by flow cytometry. $n = 3$. $^*P < 0.05$ versus kidneys 12 hours after PBS injection. (**C**) CD11b+Ly-6C+EGFP+ BM cells (1×10^6 cells/mouse) were prepared from CAG-*EGFP* mice and adoptively transferred into wild-type mice prior to a single injection of PBS or S100A8 plus S100A9 (25 μg of each) into kidneys. Transferred EGFP+ cells recruited to kidneys were analyzed by flow cytometry. Cells in R1 (CD11b+F4/80lo) were further analyzed for expression of Ly-6C and CD301.

cells within 12 hours (Figure 8B) and also induced moderate levels of apoptosis and tubular injury (Supplemental Figure 11). The controls, which included PBS, PBS containing LPS at a level matching that in the recombinant S100A8/A9 solution, or PBS whose osmolarity was matched to that of the S100A8/A9 solution using glucose, did not induce CD11b+F4/80lo cell accumulation (Figure 8B). The CD11b+F4/80hi M2-type macrophage fraction was reduced by S100A8/A9 injection, suggesting that S100A8 and S100A9 selectively recruit CD11b+F4/80lo cells to the kidneys and/or promote M1-type activation in recruited monocytes.

Previous studies have shown that CD11b+Ly-6C+ inflammatory monocytes are the major monocyte population recruited to kidneys 5 days after UUO (11). Therefore, prior to UUO we adoptively transferred BM CD11b+Ly-6C+ monocytes prepared from CAG-*EGPF* mice, in which *EGFP* was ubiquitously expressed (Supplemental Figure 12). One day after UUO, the transferred EGFP+ monocytes were recruited to the kidneys, and the majority of them exhibited the CD11b+F4/80loLy-6C+CD301− phenotype, while a minor population exhibited the CD11b+F4/80hiLy-6C−/loCD301+ M2-type phenotypes (Supplemental Figure 12A). In contrast, very few CD11b+Ly-6C− BM monocytes were recruited to UUO kidneys (data not shown). Thus, as with monocytes transferred 5 days after UUO (11), CD11b+Ly-6C+ inflammatory monocytes appear to be the major source of monocytes recruited to kidneys early after UUO. The finding that expression of *Emr1* (F4/80) and *Il1b* was increased while expression of *Csf1r* (CD115), which is highly expressed in monocytes (26), was decreased indicates that the recruited CD11b+F4/80lo cells were differentiating into M1-type macrophages. This supports the notion that kidney CD11b+F4/80lo cells include macrophages and newly recruited monocytes differentiating into macrophages.

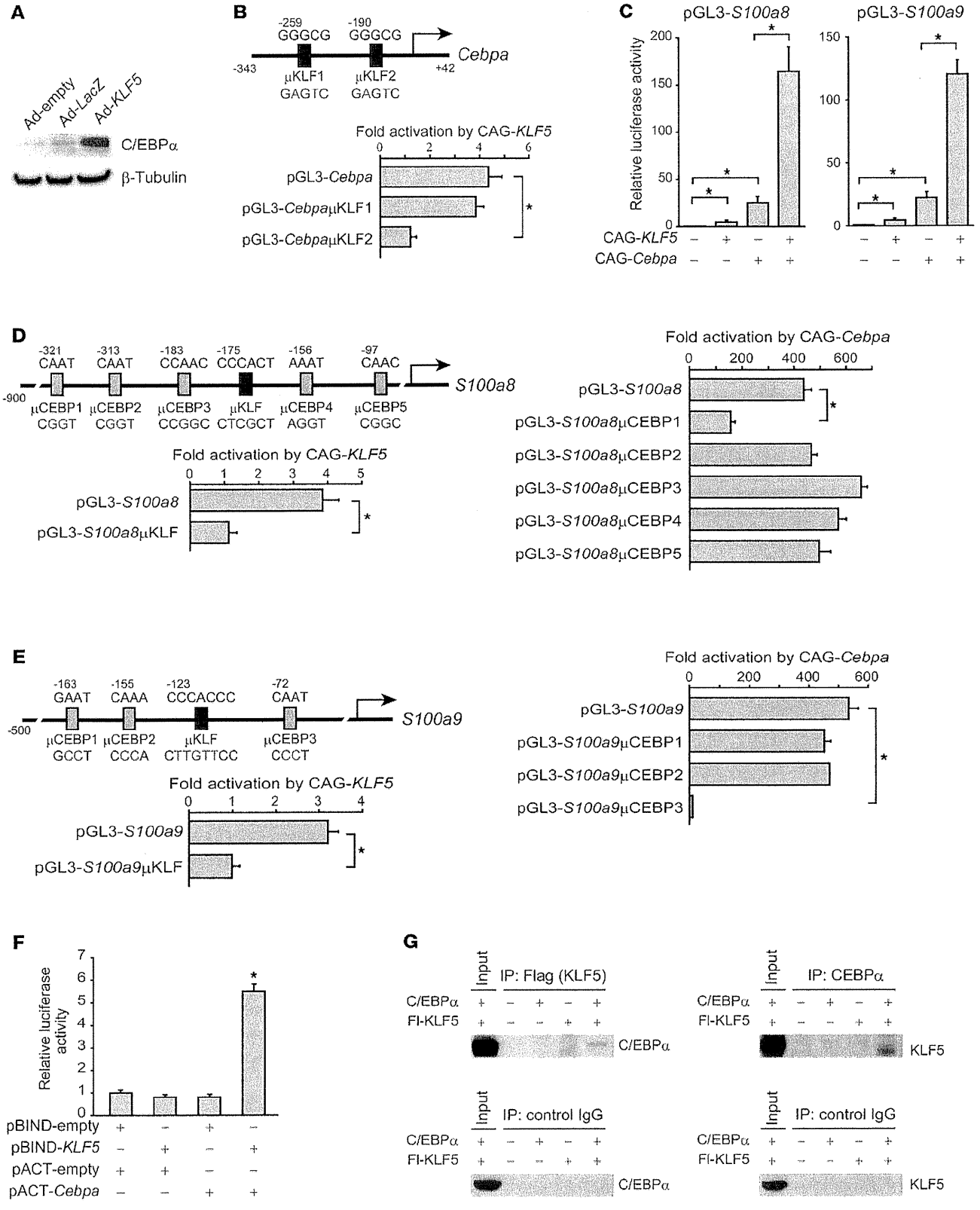
A
Ad-empty
Ad-LacZ
Ad-KLF5
C/EBPα
β-Tubulin
B
-259
GGGCG
-190
GGGCG
Cebpa
-343
+42
μKLF1
GAGTC
μKLF2
GAGTC
Fold activation by CAG-KLF5
pGL3-Cebpa
pGL3-CebpaμKLF1
pGL3-CebpaμKLF2
C
pGL3-S100a8
pGL3-S100a9
Relative luciferase activity
CAG-KLF5
CAG-Cebpa
D
-321
CAAT
-313
CAAT
-183
CCAAC
-175
CCCACT
-156
AAAT
-97
CAAC
S100a8
-900
μCEBP1
CGGT
μCEBP2
CGGT
μCEBP3
CCGGC
μKLF
CTCGCT
μCEBP4
AGGT
μCEBP5
CGGC
Fold activation by CAG-KLF5
pGL3-S100a8
pGL3-S100a8μKLF
Fold activation by CAG-Cebpa
pGL3-S100a8
pGL3-S100a8μCEBP1
pGL3-S100a8μCEBP2
pGL3-S100a8μCEBP3
pGL3-S100a8μCEBP4
pGL3-S100a8μCEBP5
E
-163
GAAT
-155
CAAA
-123
CCCACCC
-72
CAAT
S100a9
-500
μCEBP1
GCCT
μCEBP2
CCCA
μKLF
CTTGTTCC
μCEBP3
CCCT
Fold activation by CAG-KLF5
pGL3-S100a9
pGL3-S100a9μKLF
Fold activation by CAG-Cebpa
pGL3-S100a9
pGL3-S100a9μCEBP1
pGL3-S100a9μCEBP2
pGL3-S100a9μCEBP3
F
Relative luciferase activity
pBIND-empty
pBIND-KLF5
pACT-empty
pACT-Cebpa
G
Input
IP: Flag (KLF5)
C/EBPα
Fl-KLF5
C/EBPα
IP: CEBPα
KLF5
IP: control IgG
C/EBPα
KLF5

Figure 9
KLF5 transactivates the *Cebpa*, *S100a8*, and *S100a9* promoters. (**A**) Expression of C/EBPα protein in mIMCD-3 cells infected with Ad-empty, Ad-*LacZ*, or Ad-*KLF5*. (**B**) Effects of KLF5 on the activity of the *Cebpa* proximal promoter. mIMCD3 cells were transfected with *Cebpa* promoter reporter constructs containing the indicated mutations within the putative KLF5-binding sites plus either an empty (CAG-empty) or KLF5-encoding (CAG-*KLF5*) plasmid. The luciferase activity of each reporter construct cotransfected with CAG-*KLF5* was normalized to that of the reporter cotransfected with CAG-empty. Mutant sequences (indicated by μ) are shown schematically. $n = 6$. $^*P < 0.05$. (**C**) Effects of KLF5 and C/EBPα on *S100a8* and *S100a9* promoter activity. Luciferase reporters driven by the promoters were cotransfected with expression vectors for KLF5 and C/EBPα (CAG-*Cepba*), as indicated. Luciferase activity was normalized to that of the reporter construct cotransfected with CAG-empty. $n = 6$. (**D** and **E**) Relative activation of mutant *S100a8* and *S100a9* promoters by KLF5 and C/EBPα. Mutant sequences are shown schematically. $n = 6$. $^*P < 0.05$. (**F**) Mammalian two-hybrid analysis of the interaction between KLF5 and C/EBPα. mIMCD-3 cells were transfected with the indicated combinations of plasmids containing the Gal4-DNA binding domain fused to the full-length KLF5 (pBIND-*KLF5*) and the VP16-activation domain fused to the full-length C/EBPα (pACT-*Cebpa*), along with a reporter plasmid (pG5-luc). $n = 6$. $^*P < 0.05$ versus cells transfected with pBIND-empty and pACT-empty. (**G**) Physical interaction between KLF5 and C/EBPα. Lysates of mIMCD-3 cells expressing Flag-tagged KLF5 (Fl-KLF5) and C/EBPα were immunoprecipitated with antibody against Flag, C/EBPα, or control IgG. Immunoprecipitates were probed for C/EBPα or KLF5.

We next tested whether S100A8 and S100A9 might be capable of recruiting $CD11b^+Ly\text{-}6C^+$ monocytes. S100A8/A9 injection resulted in accumulation of $CD11b^+F4/80^{lo}Ly\text{-}6C^+CD301^-$ cells (Figure 8C). In contrast to UUO, S100A8/A9 injection did not induce M2-type differentiation. Following the injection, expression of *Emr1* and *Il1b* was increased, while *Csf1r* expression was decreased (Supplemental Figure 12C), indicating M1-type macrophage differentiation of recruited inflammatory monocytes in the kidneys.

We also tested whether injection of S100A8/A9 might rescue the wild-type phenotype in $Klf5^{+/-}$ kidneys. We found that S100A8/A9 increased the $CD11b^+F4/80^{lo}$ cell fractions in $Klf5^{+/-}$ kidneys to levels similar to those in wild-type kidneys, while decreasing the $CD11b^+F4/80^{hi}$ cell fraction (Supplemental Figure 13A). In addition, S100A8/A9 increased apoptosis and tubular injury, while suppressing interstitial fibrosis (Supplemental Figure 13B). Likewise, renal injury scores in $Klf5^{+/-}$ kidneys were similar to those in wild-type kidneys after S100A8/A9 injection, indicating that S100A8 and S100A9 are the key mediators regulated by KLF5 in response to UUO. Taken together, these results demonstrate that S100A8 and S100A9, which are induced by KLF5 in response to UUO, recruit $CD11b^+Ly\text{-}6C^+$ inflammatory monocytes to the kidneys and promote their M1-type differentiation in the monocytes.

KLF5 acts in concert with C/EBPα to control S100a8 and S100a9 expression. Previous in vitro studies suggest C/EBP transcription factors are involved in the control of *S100a8* and *S100a9* transcription (38–40), but it is not yet clear whether C/EBP proteins regulate the promoters in vivo. Interestingly, overexpression of *Klf5* led to increases in the expression of C/EBPα (Figure 9A and Supplemental Figure 14A), and ChIP-seq revealed that KLF5 binds to the *Cebpa* locus. Conversely, knocking down *Klf5* reduced levels of the *Cebpa* transcript and C/EBPα protein in mIMCD-3 cells (Supplemental Figure 14, B and C), suggesting KLF5 directly controls *Cebpa* expression. Consistent with this idea, a reporter plasmid containing a fragment spanning −343 to +42 bp of the *Cebpa* promoter was transactivated by KLF5 (Figure 9B). Furthermore, the *Cebpa* promoter contains two potential KLF5 binding motifs, at −259 and at −190 bp, and mutations within the motif at −190 bp abolished the KLF5-dependent transactivation.

We next conducted a series of reporter analyses to assess the functional involvement of KLF5 and C/EBPα in the transcriptional regulation of *S100a8* and *S100a9*. We found that the *S100a8* and *S100a9* promoters were transactivated by either KLF5 or C/EBPα and that their coexpression led to synergistic activation of the promoters (Figure 9C). Mutations within the potential KLF5 binding sites abolished KLF5-dependent activation of the promoters (Figure 9, D and E). Similarly, among the potential C/EBP binding sites, mutations within motifs at −321 bp of *S100a8* or −72 bp of *S100a9* significantly suppressed transactivation by C/EBPα. The synergistic transactivation of the *S100a8* and *S100a9* promoters by KLF5 and C/EBPα suggests the two transcription factors physically interact. Indeed, mammalian two-hybrid analysis showed that KLF5 and C/EBPα do interact during transcriptional regulation (Figure 9F), and coimmunoprecipitation assays showed that they physically associate with one another in mIMCD-3 cells (Figure 9G).

UUO switches KLF5 targets in vivo. To further characterize the transcriptional regulatory circuit, we used in vivo ChIP analyses to analyze the promoter binding of KLF5 and C/EBPα. Cells were isolated from renal papillae 24 hours after either UUO or control sham operation. In the control cells, KLF5 did not bind to *Cebpa*, *S100a8*, or *S100a9*, but it did bind to the *Cdh1* promoter (Figure 10A). This binding profile was reversed by UUO. Following UUO, KLF5 bound to the *Cebpa*, *S100a8*, and *S100a9* promoters, but binding to *Cdh1* was eliminated (Figure 10A). Correspondingly, whereas C/EBPα did not bind to the *S100a8* or *S100a9* promoter in control cells, it was recruited to those promoters by UUO (Figure 10B).

We then used sequential ChIP (re-ChIP) to determine whether KLF5 and C/EBPα simultaneously bind to the same promoters. Chromatin samples were prepared from renal papillary cells 12 and 24 hours after UUO: UUO induced KLF5 binding to *S100a8* and *S100a9* within 12 hours, but C/EBPα was not bound to the promoters at that time (Figure 10, C and D). The chromatin samples pulled down by KLF5 or C/EBPα antibody were then further immunoprecipitated with C/EBPα or KLF5 antibody, respectively. These re-ChIP assays showed that while C/EBPα did not bind to the KLF5-bound *S100a8* and *S100a9* promoters 12 hours after UUO (Figure 10, C and D), both KLF5 and C/EBPα were bound to the promoter 24 hours after UUO. This strongly suggests that UUO induces KLF5 binding to the *Cebpa*, *S100a8*, and *S100a9* promoters within 12 hours, and that the induction of *Cebpa* expression by KLF5 leads to cooperative transactivation of the *S100a8* and *S100a9* promoters by KLF5 and C/EBPα. As would be expected from this model, renal levels of *Klf5* transcript were increased within 4 hours after UUO, and this was followed by induction of *Cebpa* expression (Figure 11A). Levels of *S100a8*, *S100a9*, and *Ccl2* transcripts were increased within 12 hours, and levels of KLF5, C/EBPα, S100A8, and S100A9 proteins were clearly increased in whole kidneys 6–12 hours after UUO (Figure 11B). More specifically, KLF5, S100A8, and S100A9 proteins were increased in collecting duct cells 12 hours after UUO, but were undetectable in non-collecting duct cells (Figure 11C). As expected, levels of these mRNAs

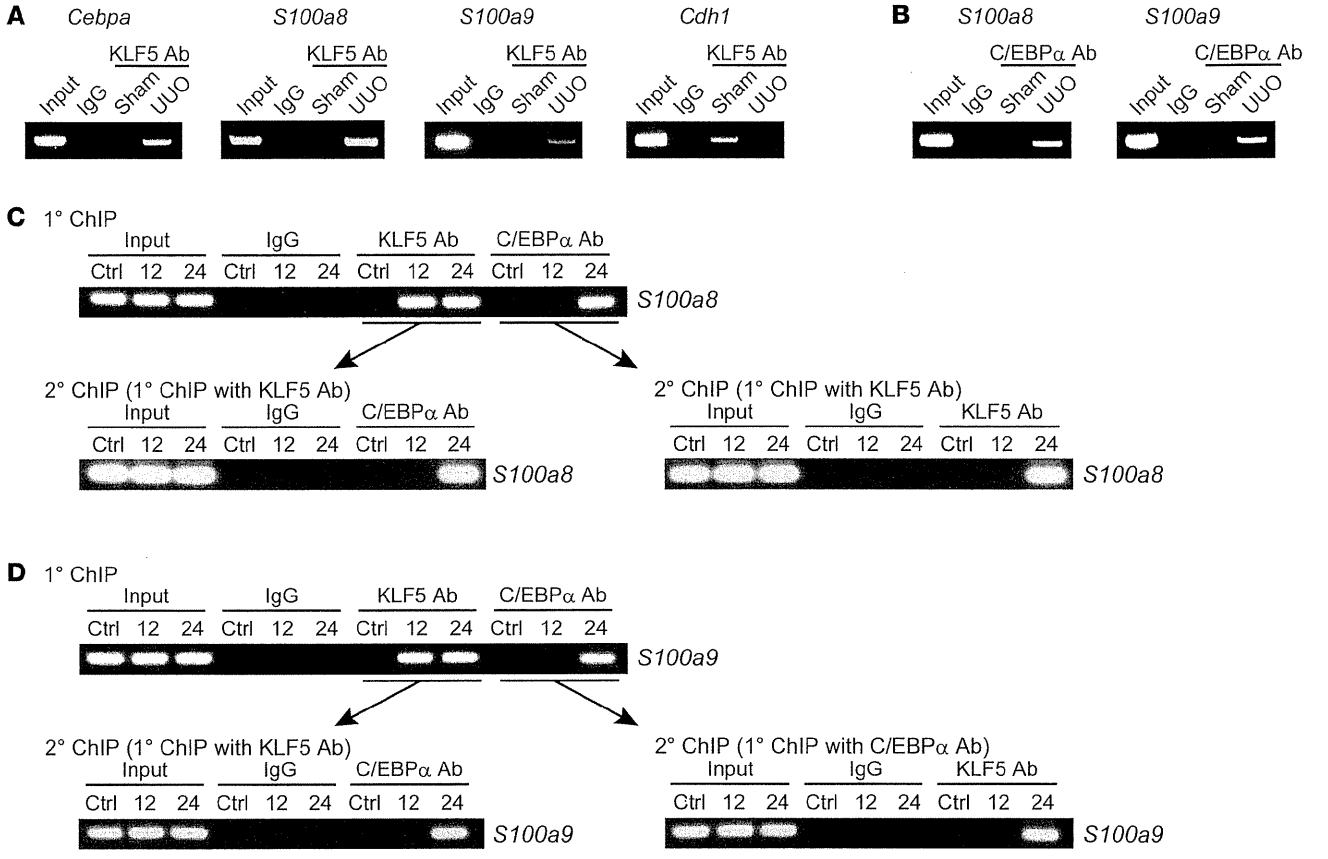

Figure 10
UUO alters KLF5 binding targets in vivo. (**A** and **B**) ChIP assays for KLF5 (**A**) and C/EBPα (**B**) binding to their target promoters in IMCD cells isolated from kidneys subjected to either UUO or sham operation. One percent of the input chromatin from IMCD cells isolated from the sham-operated kidneys was used as a positive control (Input). Samples prepared from UUO kidneys and immunoprecipitated with nonimmune IgG were used as a negative control. ChIP assays using a nontarget region (*Pdgfa* 3′UTR) as a negative control are shown in Supplemental Figure 15A. (**C** and **D**) In vivo re-ChIP analysis of the simultaneous binding of KLF5 and C/EBPα to the *S100a8* (**C**) and *S100a9* (**D**) promoters. Chromatin samples prepared from renal papillary cells of control (Ctrl) and 12- and 24-hour UUO kidneys were subjected to immunoprecipitation using KLF5 or C/EBPα antibody (1° ChIP). The immunoprecipitates were then pulled down further using C/EBPα or KLF5 antibody, respectively (2° ChIP). ChIP assays of a nontarget region (*Pdgfa* 3′UTR) are shown in Supplemental Figure 15B.

and proteins were all reduced in *Klf5*$^{+/-}$ kidneys (Figure 11, A, B, and D). By contrast, *Ccl2* expression only differed on days 4 and 7 (Figure 11A).

The binding of KLF5 to the *Cdh1* promoter under basal conditions (Figure 10A) suggests KLF5 also regulates *Cdh1* expression. That notion is supported by the observations that *Cdh1* expression was reduced in *Klf5*$^{+/-}$ kidneys (Supplemental Figure 15C), that knocking down *Klf5* reduced *Cdh1* expression in mIMCD-3 cells (Supplemental Figure 15D), and that KLF5 transactivated the *CDH1* promoter (Supplemental Figure 15E). KLF5 thus appears to control *Cdh1* expression under basal conditions, and UUO switches the KLF5 target genes from *Cdh1* to *Cebpa*, *S100a8*, and *S100a9*.

KLF5 in renal collecting duct cells plays a central role in CD11b^{+}*F4/80*^{lo} *cell accumulation and renal damage.* In the kidney, *Klf5* is primarily expressed in renal collecting ductal cells (Figure 1, A–D, and Supplemental Figure 1C). However, occasional low-level KLF5 staining was observed in a few stromal cells, which could be fibroblasts and/or BMDCs. To further establish the importance of KLF5 expressed in collecting duct cells to renal injury, we carried out a set of BM transplantation experiments. When wild-type mice whose BM had been replaced with that from either wild-type or *Klf5*$^{+/-}$ mice subjected to UUO, the CD11b^{+}F4/80^{lo} fractions did not significantly differ between the two groups (Figure 12A), nor did levels of *Klf5*, *Cebpa*, *S100a8*, and *S100a9* expression (Figure 12B) and renal injury scores (Supplemental Figure 16).

To further rule out a possible contribution of KLF5 in macrophages to the observed renal *Klf5*$^{+/-}$ phenotypes, we selectively ablated *Klf5* in myeloid cells by crossing *Klf5* floxed mice (*Klf5*$^{fl/fl}$) with *LysM-Cre* mice (41). As a result, more than 95% of *Klf5* floxed alleles were deleted in kidney CD11b^{+}F4/80^{+} cells (Supplemental Figure 17A). This *Klf5* deficiency in macrophages did not affect the accumulation of CD11b^{+}F4/80^{lo} and CD11b^{+}F4/80^{hi} cells in UUO kidneys or their expression of cytokines (Figure 7, A and B, and Supplemental Figure 17B). Moreover, renal injury scores were unaffected by myeloid-specific *Klf5* deletion (Supplemental Figure 18).

To further confirm the importance of KLF5 expressed in

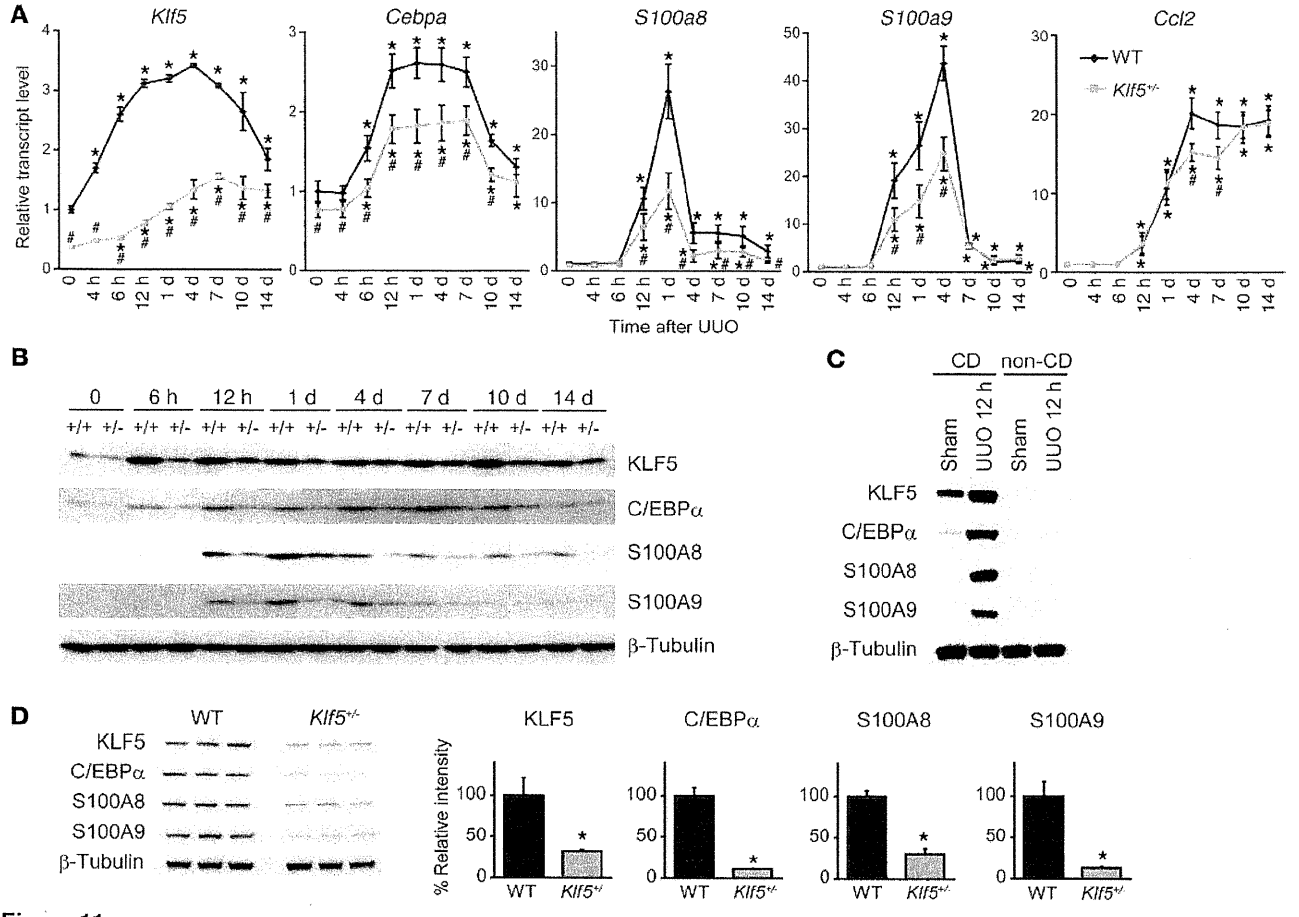

Figure 11

KLF5 is essential for induction of C/EBPα and S100A8/S100A9 in vivo. (**A**) Time course of *Klf5*, *Cebpa*, *S100a8*, *S100a9*, and *Ccl2* expression in kidneys from wild-type and *Klf5*$^{+/-}$ mice following UUO. Expression levels were normalized to those of 18s rRNA and then further normalized to the levels in the control wild-type kidney. Data labeled 0 show gene expression in kidneys under basal conditions. $n = 5$ for each group. $^{*}P < 0.05$ versus control kidneys of the same genotype; $^{\#}P < 0.05$ versus wild-type at the same time point. Note that some of the *Klf5* expression data are the same as in Figure 3A. (**B**) Time course of KLF5, C/EBPα, S100A8, and S100A9 protein expression after UUO in whole kidneys from wild-type (+/+) and *Klf5*$^{+/-}$ (+/–) mice. (**C**) Collecting duct–specific expression of KLF5, C/EBPα, S100A8, and S100A9 12 hours after UUO. KLF5, C/EBPα, S100A8, and S100A9 protein expression was analyzed in collecting duct (CD) and non–collecting duct (non-CD) cells prepared from sham-operated and 12-hour UUO kidneys. (**D**) Expression of KLF5, CEBPα, S100A8, and S100A9 proteins in CD cells isolated from wild-type and *Klf5*$^{+/-}$ kidneys 1 day after UUO. Relative intensities of the bands analyzed by quantitative densitometry are shown. $^{*}P < 0.05$ versus wild-type. $n = 3$.

the collecting duct, we selectively deleted *Klf5* from collecting duct cells by crossing *Klf5*$^{fl/fl}$ mice with *Aqp2-Cre* mice in which *Cre* expression was selectively driven in collecting duct cells by the *Aqp2* promoter (Supplemental Figure 19A). The efficacy of the *Klf5* deletion from collecting duct cells was approximately 70% (Supplemental Figure 19, B–D). Under basal conditions, *Klf5*$^{fl/fl}$;*Aqp2-Cre* mice did not show abnormal kidney histology or blood chemistry (i.e., creatinine and electrolyte levels) (Supplemental Figure 19E and Supplemental Table 4). In kidneys from the collecting duct–specific *Klf5*-knockout mice, accumulation of CD11b^{+}F4/80^{lo} cells (Figure 12C) and expression of *Klf5*, *Cebpa*, *S100a8*, and *S100a9* were significantly reduced, as compared with kidneys from *Klf5*$^{fl/fl}$ mice, 24 hours after UUO (Figure 12D). The apoptotic cell fractions and glomerular sclerosis and tubular injury scores were all reduced in *Klf5*$^{fl/fl}$;*Aqp2-Cre* mice, while interstitial fibrosis was enhanced, as compared with *Klf5*$^{fl/fl}$ mice (Supplemental Figure 18). Overall, the renal phenotypes of *Klf5*$^{fl/fl}$;*Aqp2-Cre* mice were largely comparable to those of *Klf5*$^{+/-}$ mice, indicating that KLF5 expressed in collecting duct cells is primarily responsible for the renal phenotypes observed in *Klf5*$^{+/-}$ mice and is essential for renal responses to UUO.

Discussion

The results of the present study demonstrate that renal collecting duct cells play a pivotal role in the response to renal injury (Figure 12E). In response to UUO, *S100a8* and *S100a9* expression is induced by KLF5. S100A8 and S100A9 in turn recruit CD11b^{+}Ly-6C^{+} inflammatory monocytes to the kidneys, and then contribute to the cells' differentiation into M1-type CD11b^{+}F4/80^{lo} cells, which promote renal epithelial injury and inflammation. Thereafter, the numbers of CD11b^{+}F4/80^{hi} M2-type cells, which promote fibrosis, gradually increase. As such, KLF5 is a pivotal regulator of the

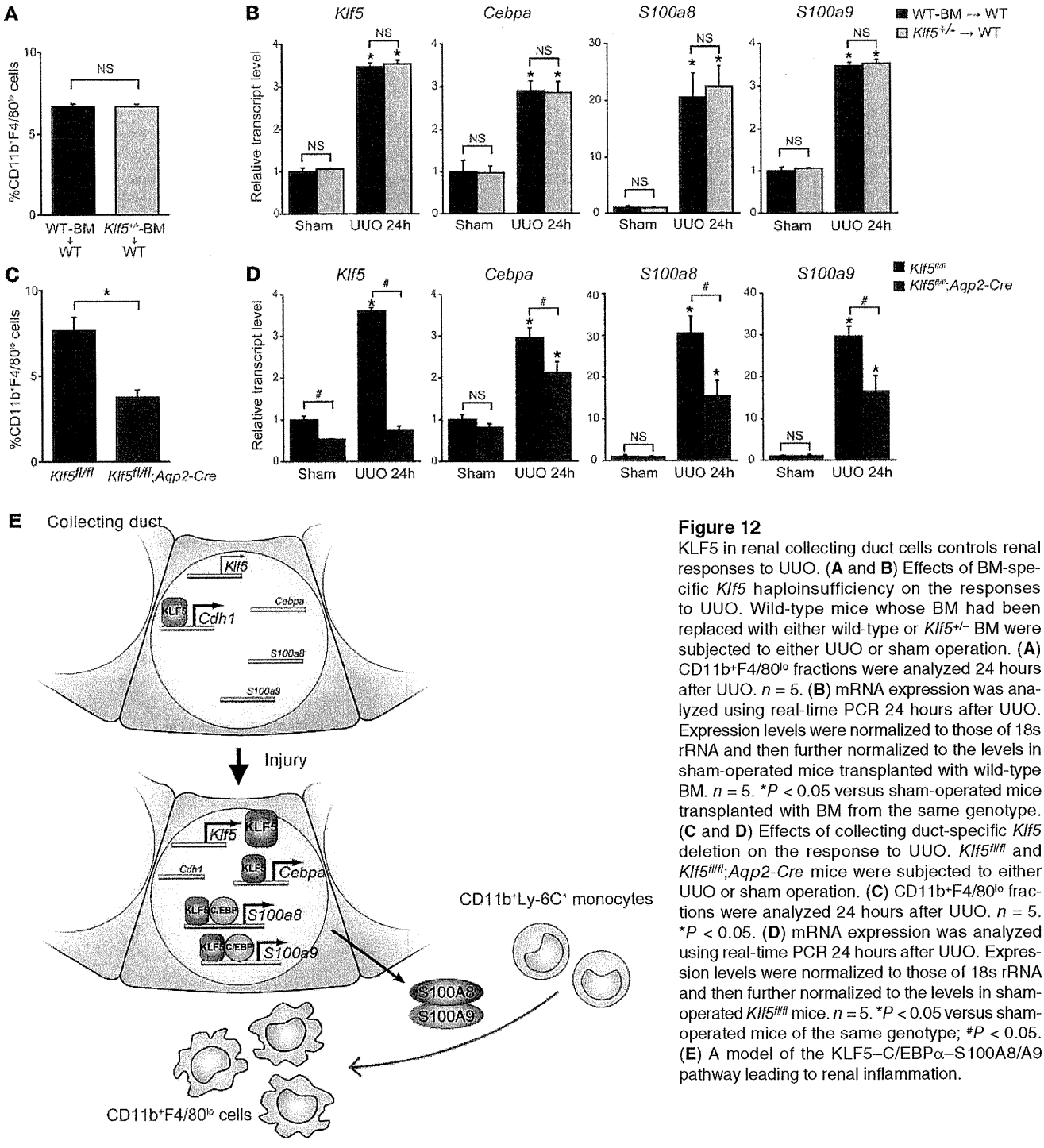

Figure 12

KLF5 in renal collecting duct cells controls renal responses to UUO. (**A** and **B**) Effects of BM-specific *Klf5* haploinsufficiency on the responses to UUO. Wild-type mice whose BM had been replaced with either wild-type or *Klf5*$^{+/-}$ BM were subjected to either UUO or sham operation. (**A**) CD11b^{+}F4/80^{lo} fractions were analyzed 24 hours after UUO. $n = 5$. (**B**) mRNA expression was analyzed using real-time PCR 24 hours after UUO. Expression levels were normalized to those of 18s rRNA and then further normalized to the levels in sham-operated mice transplanted with wild-type BM. $n = 5$. $^{*}P < 0.05$ versus sham-operated mice transplanted with BM from the same genotype. (**C** and **D**) Effects of collecting duct-specific *Klf5* deletion on the response to UUO. *Klf5*$^{fl/fl}$ and *Klf5*$^{fl/fl}$;*Aqp2-Cre* mice were subjected to either UUO or sham operation. (**C**) CD11b^{+}F4/80^{lo} fractions were analyzed 24 hours after UUO. $n = 5$. $^{*}P < 0.05$. (**D**) mRNA expression was analyzed using real-time PCR 24 hours after UUO. Expression levels were normalized to those of 18s rRNA and then further normalized to the levels in sham-operated *Klf5*$^{fl/fl}$ mice. $n = 5$. $^{*}P < 0.05$ versus sham-operated mice of the same genotype; $^{\#}P < 0.05$. (**E**) A model of the KLF5–C/EBPα–S100A8/A9 pathway leading to renal inflammation.

response of collecting duct cells to renal injury. Because KLF5 regulates early accumulation of CD11b^{+}Ly-6C^{lo} cells in UUO kidneys, *Klf5* haploinsufficiency and collecting duct–specific *Klf5* deletion skewed macrophage differentiation toward M2, leading to amelioration of the renal injury but enhancement of the fibrosis.

Our identification of two CD11b^{+}F4/80^{+} cell subpopulations with different gene expression profiles clearly demonstrates that renal inflammation involves at least two phenotypically different monocyte/macrophage subpopulations: CD11b^{+}F4/80^{lo} monocytes/macrophages showing M1-type activation and CD11b^{+}F4/80^{hi} M2-type macrophages. In addition, we found that these subpopulations differentially accumulate over the course of the response to UUO: on days 1–4 after UUO, macrophage activation was skewed to M1-type, but at later times it was shifted toward M2-type. Lin et al. recently identified subsets of macrophages in UUO kidneys based on the surface expression of Ly-6C (11). In

their study, CD11b$^+$Ly-6C^{hi} immature macrophages exhibited M1-type activation, while CD11b$^+$Ly-6C^{lo} macrophages showed the M2-type phenotype. The gene expression profiles and surface phenotypes observed in the present study strongly suggest that CD11b$^+$F4/80^{lo} and CD11b$^+$F4/80^{hi} cells largely correspond to the CD11b$^+$Ly-6C^{hi} and CD11b$^+$Ly-6C^{lo} macrophages, respectively.

The results of the present study demonstrate that renal CD11b$^+$F4/80^{lo} and CD11b$^+$F4/80^{hi} cells differ functionally from one another. By showing that inflammatory CD11b$^+$F4/80^{lo} M1-type cell accumulation was selectively suppressed in *Klf5*$^{+/-}$ mice and that tubular injury, cellular apoptosis, and proinflammatory cytokine expression were all diminished in *Klf5*$^{+/-}$ mice, the present study demonstrates that M1-type macrophages are crucially involved in the renal injury and inflammation caused by UUO. Our results also indicate that CD11b$^+$F4/80^{lo} and CD11b$^+$F4/80^{hi} cells differentially contribute to the renal response to injury, at least in part through production of different sets of cytokines. Interestingly, fibrosis was enhanced in *Klf5*$^{+/-}$ and *Klf5*$^{fl/fl}$;*Aqp2-Cre* mice, in which CD11b$^+$F4/80^{hi} M2-type macrophage accumulation was increased but accumulation of CD11b$^+$F4/80^{lo} M1-type cells was reduced. This suggests that the skewed balance toward M2 activation in *Klf5*$^{+/-}$ mice led to the enhanced fibrosis. Histologically, however, interstitial fibrosis was apparent only on day 7; thereafter, differences in the M1/M2 ratio were no longer observed between wild-type and *Klf5*$^{+/-}$ kidneys (Figure 4B). Nonetheless, expression levels of genes involved in fibrosis, including *Col3a1*, *Fn1*, *Vim*, and *Tgfb1*, were significantly increased from day 4 in *Klf5*$^{+/-}$ kidneys (Figure 3B). The activation of fibrotic processes therefore appears to coincide with increases in the M2-type cell fractions in *Klf5*$^{+/-}$ kidneys. These findings suggest that the renal environment (e.g., skewed balance toward M2 activation, reduced expression of proinflammatory cytokines, and increased expression of TGF-β1) at early times after UUO (up to day 7) alters inflammatory processes and affects the later fibrotic phenotype. This idea is supported by our finding that on day 7 levels of *Il1b* and *Ccl2* expression were reduced in CD11b$^+$F4/80^{lo} cells in *Klf5*$^{+/-}$ kidneys, while levels of *Tgf1b* and *Il10* expression were increased in CD11b$^+$F4/80^{hi} cells (Figure 7). The finding that injection of *Klf5*$^{+/-}$ mice with S100A8 or S100A9 not only skewed the monocyte/macrophage balance toward CD11b$^+$F4/80^{lo} M1-type cells but also suppressed interstitial fibrosis (Supplemental Figure 13) also supports the model.

In earlier studies, the same renal CD11b$^+$ mononuclear cell populations were identified variously as macrophages or DCs. In the present study, we refer to CD11b$^+$F4/80^{hi} cells as macrophages because they clearly differ from classical DCs in the following ways: (a) CD11c levels are lower and F4/80 levels are higher than in classical DCs; (b) CD83 expression is absent; (c) they have a macrophage-like morphology; and (d) they can be differentiated from inflammatory monocytes (11). Similarly, Lin et al. referred to CD11b$^+$Ly-6C^{lo} cells as macrophages (11), though other groups have identified populations of kidney CD11b$^+$ cells as DCs. For example, Li et al. referred to resident CD11b$^+$F4/80^{hi} cells as DCs, based on the intermediate expression of CD11c and other DC markers, including MHCII and CD86 (27). Dong et al. identified CD11c^{int}F4/80$^+$Ly-6C$^-$ cells as F4/80$^+$ DCs and showed that the population is increased in UUO kidneys (42). And Heymann et al. described CD11c^{int}CD11b^{int} cells as resident DCs in mouse glomerulonephritis modes (43). Although the precise relationships between these cells are difficult to define due to a lack of the common reference cells (e.g., spleen cells) and differences in the flow cytometric methods used, CD11b$^+$F4/80^{hi} cells, or at least subpopulations of them, appear to overlap previously identified kidney DCs. It has been difficult to clearly distinguish between macrophages and DCs, as these closely related cells share both phenotypical and functional characteristics particularly during inflammation (44). No single marker can unambiguously distinguish DCs from macrophages, and CD11c, which has been extensively used to identify DCs, is widely expressed in macrophages. Moreover, the capacity to present antigens to T cells, which is a characteristic of DCs, has also been seen in macrophages (31). Consequently, the same cell populations in various tissues have been identified as either DCs or macrophages. In particular, whether CD11c$^+$ cells derived from circulating monocytes should be classified as DCs is a matter of debate (31, 44). In the small intestine, for instance, in addition to CD11c^{hi}CD11b$^+$CD103$^+$CX3CR1$^-$ bona fide DCs, there are Ly-6c^{hi} monocyte-derived CD11c^{int}CD11b$^+$CD103$^-$CX3CR1$^+$ cells, which appear to share at least some phenotypes with renal CD11b$^+$F4/80^{hi} cells (27) and are considered by some researchers to be DCs (34, 45). However, intestinal CX3CR1$^+$ cells do not migrate into draining mesenteric lymph nodes or efficiently present antigens to T cells (46). These characteristics of intestinal CX3CR1$^+$ cells are indistinguishable from those of tissue macrophages (44). Clearly, further study of the lineages and functions, including migratory capacity, of kidney CD11b$^+$ cells will be needed to determine whether they should be classified as macrophages or DCs.

Renal CD11c^{hi}MHCII$^+$CD83$^+$CD11b$^-$ cells closely resemble splenic classical DCs phenotypically and morphologically. An earlier study identified CD11c$^+$CD103$^+$MHCII$^+$CD11b$^-$ cells in kidneys as CD103$^+$ DCs (47), and those cells might be related to the CD11c^{hi} cells identified in the present study. However, additional studies of the function and lineage of these cells will be needed before they can be classified as renal classical DCs.

The surface phenotypes of CD11b$^+$F4/80^{lo} cells (e.g., CD11c^{lo}MHCII$^{-/+}$CD86$^-$CD83$^-$), their morphology, and the fact that they derive from inflammatory monocytes all strongly suggest they are macrophages and monocytes in the process of differentiating into macrophages. However, these cells might also have been identified as inflammatory DCs in some studies (42). In addition, we found that a minor population of CD11b$^+$F4/80^{lo} cells showed higher levels of CD11c and MHCII, particularly in normal and day-7 UUO kidneys (Supplemental Figure 6). Given that inflammatory monocytes can differentiate into CD11b$^+$F4/80^{hi} cells as well as CD11b$^+$F4/80^{lo} cells (Supplemental Figure 12 and ref. 11), they may represent intermediary cells differentiating into CD11b$^+$F4/80^{hi} M2-type cells. Future studies should address the differentiation pathways of inflammatory monocytes within kidneys and identify markers with which to trace them.

S100A8 and S100A9 are calcium-binding secretory proteins that can form homodimers and heterodimers, with the latter being more prevalent (48, 49). We found that levels of *S100a8* and *S100a9* expression peaked on days 1 and 4, respectively, after UUO (Figure 11A), at a time when CD11b$^+$F4/80^{lo} cells were accumulating within the kidneys (Figure 4B), which suggests S100A8 and S100A9 are essential for inflammatory CD11b$^+$F4/80^{lo} cell accumulation early in the response to UUO. We also found that adoptively transferred CD11b$^+$Ly-6C$^+$ inflammatory monocytes were recruited to kidneys following S100A8/A9 injection, and that the recruited cells exhibited the CD11b$^+$F4/80^{lo}Ly-6C$^+$CD206$^-$CD301$^-$ M1-type phenotype (Figure 8C). S100A8 and S100A9 were also capable of inducing M1 markers in BMDMs (Figure 8A). Collectively, these results demon-

strate that S100A8 and S100A9 are important for the recruitment of inflammatory monocytes and their subsequent differentiation into M1-type macrophages during the early response to UUO.

That the accumulation of CD11b$^+$F4/80^{hi} cells begins 4 days after UUO suggests the renal microenvironment only becomes supportive of M2 activation at later times. Consistent with this idea, we found that only a minor population of CD11b$^+$Ly-6C$^+$ monocytes acquires the M2-type phenotype when transferred prior to UUO, whereas Lin et al. showed that when transferred 5 days after UUO, major populations of CD11b$^+$Ly-6C$^+$ monocytes exhibit the M2-type phenotype (11). Because S100A8/A9 expression declines, it is likely that other cytokines recruit monocytes to kidneys at later times after UUO. MCP-1 (CCL2) is one candidate chemokine for such later recruitment (Figure 11A). Although we favor a model in which proinflammatory monocytes differentiate into at least two types of macrophages in response to the kidney microenvironment, the fact that monocytes appear to be recruited by different signals at different times suggests there are multiple subsets CD11b$^+$Ly-6C$^+$ inflammatory monocytes that are differentially recruited to kidneys and might differ in the direction of their differentiation (25).

The results obtained with *Klf5$^{fl/fl}$;Aqp2-Cre* mice demonstrate that expression of KLF5 in collecting duct epithelial cells is essential for the renal response to UUO. However, KLF5 might also have functions in other cell types, including macrophages and fibroblasts. Results obtained after transplantation of *Klf5$^{+/-}$* BM and in *Klf5$^{fl/fl}$;LysM-Cre* mice indicate that, even if KLF5 were functionally active in macrophages, its cell-autonomous function in macrophages would not be important for the renal *Klf5$^{+/-}$* phenotypes. Indeed, the reduced expression of *Il1b* and *Ccl2* in CD11b$^+$F4/80^{lo} cells and increased expression of *Tgfb1* and *Il10* in CD11b$^+$F4/80^{hi} cells in *Klf5$^{+/-}$* mice, but not *Klf5$^{fl/fl}$;LysM-Cre* mice (Figure 7, A and B), is indicative of the importance of cell non-cell-autonomous effects on macrophage activation in *Klf5$^{+/-}$* kidneys. Fibroblasts are another important cell type involved in mediating tubulointerstitial damage, and we previously showed that KLF5 expressed in cardiac fibroblasts is important for the cardiac responses to pressure overload (18). In kidneys the level of *Klf5* expression in α-SMA$^+$ myofibroblasts, mesangial cells, and smooth muscle cells was significantly lower than in cardiac fibroblasts (Supplemental Figure 1C). Moreover, if the functions of KLF5 in renal fibroblasts are similar to those in cardiac fibroblasts, *Klf5* haploinsufficiency in renal fibroblasts would reduce fibrosis. It is therefore unlikely that cell-autonomous alterations of fibroblast function due to *Klf5* haploinsufficiency make a major contribution to the renal *Klf5$^{+/-}$* phenotypes. The results of the present study thus indicate that the observed renal *Klf5$^{+/-}$* phenotypes primarily reflect *Klf5* haploinsufficiency in the collecting duct.

Our data show that collecting duct epithelial cells are the major sensor of stress elicited by UUO. One important question remaining is, what do those cells sense? Given that *Klf5* expression was increased within 4 hours after UUO, and KLF5 bound to the *S100a8* and *S100a9* promoters within 12 hours, at a time when structural changes were minimal, it is very unlikely that pelvic dilation is the cause. One attractive candidate is mechanical force. After UUO there is a sudden rise in ureteric and intrarenal pressure, which translates into tubular mechanical stretch (50). Although very little is known about the effects of mechanical stretch on collecting duct epithelial cells, mechanical stretch is known to profoundly affect the function in various cell types (51). On the other hand, many other factors, including proteinuria, hypoxia, oxidative stress, and glomerulus-derived cytokines, likely contribute to activation of collecting duct cells (3). In that regard, we recently found that reactive oxygen species induce *Klf5* expression in smooth muscle cells (52). Much work will be needed to clarify the mechanism by which collecting duct epithelial cells are activated under various disease conditions. Nevertheless, the results of the present study clearly indicate that the collecting duct is an essential regulator of inflammatory processes in the kidney, and the molecular mechanism identified in the present study may provide attractive targets for novel therapeutic strategies.

Methods

Mice. Male C57BL6/6J mice were purchased from CLEA Japan and maintained on a standard mouse chow diet. *Klf5$^{+/-}$* and *Klf5$^{fl/fl}$* mice were generated as described previously (17, 18). *Aqp2-Cre* mice were purchased from The Jackson Laboratory. UUO was performed as described previously (53). For BM transplantation, 8-week-old mice were lethally irradiated, and the next day unfractionated BM cells were administered to each recipient mouse. See Supplemental Methods for details. For renal function analysis, reversible UUO was performed (22). Briefly, 12-week-old mice were anesthetized and the right ureter was then ligated. After 3 days the right ureter ligation was removed, and the mice were allowed to recover for 7 days before the left ureter was ligated. All experiments were approved by the University of Tokyo Ethics Committee for Animal Experiments and strictly adhered to the guidelines for animal experiments of the University of Tokyo.

Flow cytometric analysis. The methods used to prepare cells from kidneys were described previously (54). All flow cytometric analyses were performed using a FACScalibur (BD) and FlowJo software (Tree Star). Cells were sorted using a FACSaria II (BD). See Supplemental Methods for details.

ChIP assays. ChIP assays were carried out as described previously (19). ChIP-seq was performed by sequencing the immunoprecipitated DNA using a 454 sequencer (Roche Diagnostics), after which the sequence reads were mapped to the reference mouse genome. See Supplemental Methods for details of in vivo ChIP and re-ChIP assays.

Infusion of recombinant proteins into kidney. Human recombinant S100A8 and A100A9 were purchased from ProtEra and dissolved in PBS (0.5 mg/ml). The LPS level in the mixed S100A8 and S100A9 solution was analyzed using a limulus amoebocyte lysate assay (Seikagaku Biobusiness Corp.). As solution of LPS in PBS in which the LPS concentration was matched to that in the S100A8/A9 solution (0.092 EU/ml) served as a control. An isotonic solution of glucose in PBS and PBS alone were also used as controls. A mixture of S100A8 and S100A9 (25 μg each) was injected into the parenchyma of the left kidney without vascular clamping. The total injected volume for one kidney was 50 μl.

Statistics. Comparisons between 2 groups were made using Student's *t* test (2-tailed). Differences among more than 2 groups were analyzed using 1-way ANOVA followed by Bonferroni (3 groups) or Tukey-Kramer post hoc (>4 groups) tests. *P* values less than 0.05 were considered significant. Error bars represent SD except where otherwise indicated.

Acknowledgments

We gratefully acknowledge M. Hayashi, N. Yamanaka, A. Ono, X. Yingda, Y. Tani, and E. Magoshi for their excellent technical assistance. We would like to thank Carey Lumeng for valuable discussion. This study was supported in part by the Funding Program for World-Leading Innovative R&D on Science and Technology (FIRST Program) from the Japan Society for the Promotion of Science (to R. Nagai); grants-in-aid from the Ministry of Education, Culture, Sports, Science and Technology, Japan (to R. Nagai, I. Manabe, and

K. Fujiu); a grant for Translational Systems Biology and Medicine Initiative from the Ministry of Education, Culture, Sports, Science and Technology of Japan and a research grant from the National Institute of Biomedical Innovation (to R. Nagai); and research grants from the Japan Science and Technology Institute, the Sumitomo Foundation, Takeda Science Foundation, the Mochida Memorial Foundation for Medical and Pharmaceutical Research, and the Mitsubishi Pharma Research Foundation (to I. Manabe).

Received for publication February 14, 2011, and accepted in revised form June 8, 2011.

Address correspondence to: Ichiro Manabe or Ryozo Nagai, Department of Cardiovascular Medicine, University of Tokyo, 7-3-1, Hongo, Bunkyo, Tokyo 113-8655, Japan. Phone: 81.3.3815.6672; Fax: 81.3.3818.6673; E-mail: manabe-tky@umin.ac.jp (I. Manabe), nagai-tky@umin.ac.jp (R. Nagai).

1. Harris RC, Neilson EG. Toward a unified theory of renal progression. *Annu Rev Med.* 2006;57:365–380.
2. Chevalier RL, Forbes MS, Thornhill BA. Ureteral obstruction as a model of renal interstitial fibrosis and obstructive nephropathy. *Kidney Int.* 2009;75(11):1145–1152.
3. Sean Eardley K, Cockwell P. Macrophages and progressive tubulointerstitial disease. *Kidney Int.* 2005;68(2):437–455.
4. Schnaper HW, Kopp JB. Why kidneys fail: report from an American Society of Nephrology advances in research conference. *J Am Soc Nephrol.* 2006;17(7):1777–1781.
5. Kluth DC, Erwig L-P, Rees AJ. Multiple facets of macrophages in renal injury. *Kidney Int.* 2004;66(2):542–557.
6. Ricardo SD, van Goor H, Eddy AA. Macrophage diversity in renal injury and repair. *J Clin Invest.* 2008;118(11):3522–3530.
7. Kluth DC. Pro-resolution properties of macrophages in renal injury. *Kidney Int.* 2007;72(3):234–236.
8. Duffield JS, et al. Selective depletion of macrophages reveals distinct, opposing roles during liver injury and repair. *J Clin Invest.* 2005;115(1):56–65.
9. Mosser DM, Edwards JP. Exploring the full spectrum of macrophage activation. *Nat Rev Immunol.* 2008;8(12):958–969.
10. Mantovani A. Macrophage diversity and polarization: in vivo veritas. *Blood.* 2006;108(2):408–409.
11. Lin SL, Castano AP, Nowlin BT, Lupher ML Jr, Duffield JS. Bone marrow Ly6Chigh monocytes are selectively recruited to injured kidney and differentiate into functionally distinct populations. *J Immunol.* 2009;183(10):6733–6743.
12. Fenton RA, Knepper MA. Mouse models and the urinary concentrating mechanism in the new millennium. *Physiol Rev.* 2007;87(4):1083–1112.
13. Ivanova L, Butt MJ, Matsell DG. Mesenchymal transition in kidney collecting duct epithelial cells. *Am J Physiol Renal Physiol.* 2008;294(5):F1238–F1248.
14. Smith JP, Pozzi A, Dhawan P, Singh AB, Harris RC. Soluble HB-EGF induces epithelial-to-mesenchymal transition in inner medullary collecting duct cells by upregulating Snail-2. *Am J Physiol Renal Physiol.* 2009;296(5):F957–F965.
15. Butt MJ, Tarantal AF, Jimenez DF, Matsell DG. Collecting duct epithelial-mesenchymal transition in fetal urinary tract obstruction. *Kidney Int.* 2007;72(8):936–944.
16. Haldar SM, Ibrahim OA, Jain MK. Kruppel-like factors (KLFs) in muscle biology. *J Mol Cell Cardiol.* 2007;43(1):1–10.
17. Shindo T, et al. Kruppel-like zinc-finger transcription factor KLF5/BTEB2 is a target for angiotensin II signaling and an essential regulator of cardiovascular remodeling. *Nat Med.* 2002;8(8):856–863.
18. Takeda N, et al. Cardiac fibroblasts are essential for the adaptive response of the murine heart to pressure overload. *J Clin Invest.* 2010;120(1):254–265.
19. Fujiu K, et al. Synthetic retinoid Am80 suppresses smooth muscle phenotypic modulation and in-stent neointima formation by inhibiting KLF5. *Circ Res.* 2005;97(11):1132–1141.
20. Nelson RD, et al. Expression of an AQP2 Cre recombinase transgene in kidney and male reproductive system of transgenic mice. *Am J Physiol Cell Physiol.* 1998;275(1 pt 1):C216–C226.
21. Bascands JL, Schanstra JP. Obstructive nephropathy: insights from genetically engineered animals. *Kidney Int.* 2005;68(3):925–937.
22. Puri TS, et al. Chronic kidney disease induced in mice by reversible unilateral ureteral obstruction is dependent on genetic background. *Am J Physiol Renal Physiol.* 2010;298(4):F1024–F1032.
23. Medzhitov R. Origin and physiological roles of inflammation. *Nature.* 2008;454(7203):428–435.
24. Zhu B, et al. CD11b+Ly-6C(hi) suppressive monocytes in experimental autoimmune encephalomyelitis. *J Immunol.* 2007;179(8):5228–5237.
25. Swirski FK, et al. Ly-6Chi monocytes dominate hypercholesterolemia-associated monocytosis and give rise to macrophages in atheromata. *J Clin Invest.* 2007;117(1):195–205.
26. Geissmann F, Manz MG, Jung S, Sieweke MH, Merad M, Ley K. Development of monocytes, macrophages, and dendritic cells. *Science.* 2010;327(5966):656–661.
27. Li L, et al. The chemokine receptors CCR2 and CX3CR1 mediate monocyte/macrophage trafficking in kidney ischemia-reperfusion injury. *Kidney Int.* 2008;74(12):1526–1537.
28. Krüger T, et al. Identification and functional characterization of dendritic cells in the healthy murine kidney and in experimental glomerulonephritis. *J Am Soc Nephrol.* 2004;15(3):613–621.
29. Dong X, Swaminathan S, Bachman LA, Croatt AJ, Nath KA, Griffin MD. Resident dendritic cells are the predominant TNF-secreting cell in early renal ischemia-reperfusion injury. *Kidney Int.* 2007;71(7):619–628.
30. Hochheiser K, Tittel A, Kurts C. Kidney dendritic cells in acute and chronic renal disease. *Int J Exp Pathol.* 2011;92(3):193–201.
31. Hume DA. Macrophages as APC and the dendritic cell myth. *J Immunol.* 2008;181(9):5829–5835.
32. Prechtel A, Steinkasserer A. CD83: an update on functions and prospects of the maturation marker of dendritic cells. *Arch Dermatol Res.* 2007;299(2):59–69.
33. Vakkila J, Lotze MT, Riga C, Jaffe R. A basis for distinguishing cultured dendritic cells and macrophages in cytospins and fixed sections. *Pediatr Dev Pathol.* 2005;8(1):43–51.
34. Pabst O, Bernhardt G. The puzzle of intestinal lamina propria dendritic cells and macrophages. *Eur J Immunol.* 2010;40(8):2107–2111.
35. Liu Y, et al. Unique expression of suppressor of cytokine signaling 3 is essential for classical macrophage activation in rodents in vitro and in vivo. *J Immunol.* 2008;180(9):6270–6278.
36. Vandal K, Rouleau P, Boivin A, Ryckman C, Talbot M, Tessier PA. Blockade of S100A8 and S100A9 suppresses neutrophil migration in response to lipopolysaccharide. *J Immunol.* 2003;171(5):2602–2609.
37. Ryckman C, Vandal K, Rouleau P, Talbot M, Tessier PA. Proinflammatory activities of S100: proteins S100A8, S100A9, and S100A8/A9 induce neutrophil chemotaxis and adhesion. *J Immunol.* 2003;170(6):3233–3242.
38. Endoh Y, Chung YM, Clark IA, Geczy CL, Hsu K. IL-10-dependent S100A8 gene induction in monocytes/macrophages by double-stranded RNA. *J Immunol.* 2009;182(4):2258–2268.
39. Nacken W, Lekstrom-Himes JA, Sorg C, Manitz MP. Molecular analysis of the mouse S100A9 gene and evidence that the myeloid specific transcription factor C/EBPepsilon is not required for the regulation of the S100A9/A8 gene expression in neutrophils. *J Cell Biochem.* 2001;80(4):606–616.
40. Kuwayama A, Kuruto R, Horie N, Takeishi K, Nozawa R. Appearance of nuclear factors that interact with genes for myeloid calcium binding proteins (MRP-8 and MRP-14) in differentiated HL-60 cells. *Blood.* 1993;81(11):3116–3121.
41. Clausen BE, Burkhardt C, Reith W, Renkawitz R, Förster I. Conditional gene targeting in macrophages and granulocytes using LysMcre mice. *Transgenic Res.* 1999;8(4):265–277.
42. Dong X, Bachman LA, Miller MN, Nath KA, Griffin MD. Dendritic cells facilitate accumulation of IL-17 T cells in the kidney following acute renal obstruction. *Kidney Int.* 2008;74(10):1294–1309.
43. Heymann F, et al. Kidney dendritic cell activation is required for progression of renal disease in a mouse model of glomerular injury. *J Clin Invest.* 2009;119(5):1286–1297.
44. Geissmann F, Gordon S, Hume DA, Mowat AM, Randolph GJ. Unravelling mononuclear phagocyte heterogeneity. *Nat Rev Immunol.* 2010;10(6):453–460.
45. Varol C, et al. Intestinal lamina propria dendritic cell subsets have different origin and functions. *Immunity.* 2009;31(3):502–512.
46. Schulz O, et al. Intestinal CD103+, but not CX3CR1+, antigen sampling cells migrate in lymph and serve classical dendritic cell functions. *J Exp Med.* 2009;206(13):3101–3114.
47. Ginhoux F, et al. The origin and development of nonlymphoid tissue CD103+ DCs. *J Exp Med.* 2009;206(13):3115–3130.
48. Nacken W, Roth J, Sorg C, Kerkhoff C. S100A9/S100A8: myeloid representatives of the S100 protein family as prominent players in innate immunity. *Microsc Res Tech.* 2003;60(6):569–580.
49. Gebhardt C, Németh J, Angel P, Hess J. S100A8 and S100A9 in inflammation and cancer. *Biochem Pharmacol.* 2006;72(11):1622–1631.
50. Quinlan MR, Docherty NG, Watson RWG, Fitzpatrick JM. Exploring mechanisms involved in renal tubular sensing of mechanical stretch following ureteric obstruction. *Am J Physiol Renal Physiol.* 2008;295(1):F1–F11.
51. Jaalouk DE, Lammerding J. Mechanotransduction gone awry. *Nat Rev Mol Cell Biol.* 2009;10(1):63–73.
52. Oishi Y, et al. Regulatory polymorphism in transcription factor KLF5 at the MEF2 element alters the response to angiotensin II and is associated with human hypertension. *FASEB J.* 2010;24(6):1780–1788.
53. Ophascharoensuk V, et al. Obstructive uropathy in the mouse: role of osteopontin in interstitial fibrosis and apoptosis. *Kidney Int.* 1999;56(2):571–580.
54. Vielhauer V, Anders HJ, Perez de Lema G, Luckow B, Schlondorff D, Mack M. Phenotyping renal leukocyte subsets by four-color flow cytometry: characterization of chemokine receptor expression. *Nephron Exp Nephrol.* 2003;93(2):e63.

JEM

Article

G-CSF influences mouse skeletal muscle development and regeneration by stimulating myoblast proliferation

Mie Hara,[1] Shinsuke Yuasa,[1,2] Kenichiro Shimoji,[1] Takeshi Onizuka,[1] Nozomi Hayashiji,[1] Yohei Ohno,[1] Takahide Arai,[1] Fumiyuki Hattori,[1] Ruri Kaneda,[1] Kensuke Kimura,[1] Shinji Makino,[1,2] Motoaki Sano,[1] and Keiichi Fukuda[1]

[1]Department of Cardiology and [2]Center for Integrated Medical Research, Keio University School of Medicine, Shinjuku, Tokyo 160-8582, Japan

The Journal of Experimental Medicine

After skeletal muscle injury, neutrophils, monocytes, and macrophages infiltrate the damaged area; this is followed by rapid proliferation of myoblasts derived from muscle stem cells (also called satellite cells). Although it is known that inflammation triggers skeletal muscle regeneration, the underlying molecular mechanisms remain incompletely understood. In this study, we show that granulocyte colony-stimulating factor (G-CSF) receptor (G-CSFR) is expressed in developing somites. G-CSFR and G-CSF were expressed in myoblasts of mouse embryos during the midgestational stage but not in mature myocytes. Furthermore, G-CSFR was specifically but transiently expressed in regenerating myocytes present in injured adult mouse skeletal muscle. Neutralization of endogenous G-CSF with a blocking antibody impaired the regeneration process, whereas exogenous G-CSF supported muscle regeneration by promoting the proliferation of regenerating myoblasts. Furthermore, muscle regeneration was markedly impaired in G-CSFR–knockout mice. These findings indicate that G-CSF is crucial for skeletal myocyte development and regeneration and demonstrate the importance of inflammation-mediated induction of muscle regeneration.

CORRESPONDENCE
Keiichi Fukuda:
kfukuda@sc.itc.keio.ac.jp

Abbreviations used: APRE, acute phase response element; EGFP, enhanced GFP; ERK, extracellular regulated kinase; G-CSFR, G-CSF receptor; JNK, c-Jun N-terminal kinase; MRF, myogenic regulatory factor.

Adult skeletal muscle has resident stem cells, called satellite cells, which are responsible for generating new muscle under both physiological and pathophysiologic conditions. Although these muscles have the capacity to regenerate, this capacity has some limitations (Le Grand and Rudnicki, 2007). There are several skeletal muscle diseases such as skeletal muscle dystrophy, myopathy, severe injury, and disuse syndrome for which there are no effective treatments (Shi and Garry, 2006). Although several studies have identified various growth factors and cytokines that regulate skeletal muscle development and regeneration, effective control of regeneration hasn't been achieved using these factors in the clinical setting (Buckingham and Montarras, 2008). Therefore, it is worth elucidating the mechanisms of skeletal muscle regeneration and developing novel regeneration therapies.

After injury to skeletal muscle, neutrophils, monocytes, and macrophages infiltrate the damaged area. Concomitantly, satellite cells differentiate into transient-amplifying myoblasts, which rapidly proliferate, fuse with one another, and regenerate skeletal myotubes. During these processes, inflammation and regeneration are tightly linked. Therefore, it is reasonable to assume that some factors expressed during the inflammatory process influence skeletal muscle regeneration. However, the precise mechanisms remain unknown.

Previously, when we looked for potent differentiation-promoting factors during embryonic stem cell differentiation (Yuasa et al., 2005, 2010), we noted a marked elevation in the expression of G-CSF receptor (G-CSFR; encoded

M. Hara and S. Yuasa contributed equally to this paper.

The Rockefeller University Press $30.00
J. Exp. Med. Vol. 208 No. 4 715-727
www.jem.org/cgi/doi/10.1084/jem.20101059

by *csf3r*) in developing cardiomyocytes (Shimoji et al., 2010). Interestingly, we also found a marked increase in G-CSFR expression in developing somites. G-CSF was initially identified as a hematopoietic cytokine and has been used in both basic research studies and in the clinic for the mobilization of hematopoietic stem cells (Demetri and Griffin, 1991; Welte et al., 1996; Metcalf, 2008). However, recently, studies suggest that G-CSF also plays roles in cell differentiation, proliferation, and survival (Avalos, 1996; Harada et al., 2005; Zaruba et al., 2009). These findings encouraged us to investigate the involvement of G-CSF and G-CSFR in skeletal myocyte development and regeneration and to examine the link between inflammation and regeneration.

In this study, we show that skeletal myoblasts express G-CSF/G-CSFR and proliferate in an autocrine fashion in skeletal myocyte development. We also show that both infiltrating inflammatory cell–derived G-CSF and externally administered G-CSF enhance skeletal myoblast proliferation and facilitate skeletal muscle regeneration.

RESULTS

csf3r is expressed in the developing somite

Initially, we investigated the *csf3r* expression in the developing mouse embryo. Whole-mount in situ hybridization revealed that *csf3r* was expressed in the somite of the embryonic day (E) 9.5 mouse embryo. To localize *csf3r* expression within the somites, we used several markers of skeletal myocyte differentiation (Fig. 1 a). The *c-met* gene, which encodes a receptor for hepatocyte growth factor, is expressed in the dermomyotome and is essential for the delamination/migration of muscle progenitor cells (Yang et al., 1996). The expression of *c-met* was restricted to the ventral portion of the somite, and the expression pattern of *csf3r* wasn't similar to that of *c-met*. Skeletal myocyte development is finely regulated by myogenic transcription factors. *pax3* is first expressed in the presomitic mesoderm and is expressed in the somitic epithelium of the dermomyotome (Jostes et al., 1990; Bober et al., 1994). *pax3* is repressed as dermomyotome-derived cells activate myogenic transcription factors. The expression pattern of *pax3* was different from that of *csf3r*. The myogenic bHLH (basic helix-loop-helix) genes also show unique expression patterns in different skeletal muscle developmental stages. *myoD* and *myf5* are expressed in undifferentiated proliferating myoblasts (Tapscott et al., 1988; Venters et al., 1999), whereas *mrf4* isn't expressed until a late stage in the differentiation program (Rhodes and Konieczny, 1989; Bober et al., 1991). Compared with these marker expression patterns, the *csf3r* expression pattern resembled those of *myf5* and *myoD*. The expression pattern of the late differentiation marker *mrf4* wasn't identical to that of *csf3r*.

Immunofluorescence staining of sections of embryos of different developing stages demonstrated that G-CSFR expression in the somite was restricted to the E9.5–10.5 period; before E9.5, G-CSFR wasn't observed in the somite, and by E11.5, G-CSFR expression had disappeared (Fig. 1 b). These results indicate that G-CSF is involved in the development of undifferentiated proliferating myoblasts.

G-CSF and G-CSFR are expressed in differentiating skeletal myocytes

Immunostaining for markers of several differentiation stages revealed the stage at which skeletal myocytes expressed the G-CSFR. Skeletal muscle progenitor cells arise in the central part of the dermomyotome, coexpress Pax3 and Pax7, and can differentiate into skeletal muscle fibers during embryogenesis (Messina and Cossu, 2009). Pax3 and Pax7 have partially overlapping and partially distinct functions in myogenic progenitor cells and are both down-regulated during myogenic differentiation, after myogenic regulatory factor (MRF) expression. The Pax3- and Pax7-expressing myogenic progenitor cells didn't express G-CSFR (Fig. 1 c). However, the cells with declining levels of Pax3 and Pax7, which started to express MyoD and myogenin, showed G-CSFR expression (Fig. 1 d). In agreement with a previous study on the G-CSFR expression pattern, the immunoreactivity for G-CSFR was localized to the cell membrane and cytoplasm under steady-state conditions (Aarts et al., 2004). These cells also expressed desmin, which is an intermediate filament expressed in skeletal muscle (Fig. 1 d).

G-CSF expression was also examined by immunostaining. G-CSF expression wasn't detected in the Pax3- and Pax7-expressing myogenic progenitor cells (Fig. 1 e). As seen for the G-CSFR–expressing cells, the cells with declining levels of Pax3 and Pax7, which started to express MyoD and myogenin, showed G-CSF expression (Fig. 1 f). Double immunostaining for G-CSF and G-CSFR revealed that the G-CSFR–expressing cells also expressed G-CSF. These results indicate that early skeletal myocyte differentiating cells undergo autocrine G-CSF signaling in the developing myoblasts.

G-CSF promotes myoblast proliferation in vitro

To elucidate the role of G-CSF in myogenic cells, myoblast cells were analyzed in vitro. The C2C12 cell line is a subclone of C2 cells, which were established from the regenerating thigh muscle of an adult mouse and which are widely used as a myoblast cell line (Blau et al., 1983). In low-serum conditions, C2C12 cells differentiate and fuse with each other to form multinucleated myotubes (Fig. 2 a). Immunostaining for G-CSFR and α-actinin revealed that the premature C2C12 cells expressed G-CSFR but not actinin, whereas the mature fused myotubes clearly expressed α-actinin, and the α-actinin–positive cells never expressed G-CSFR. Western blot analysis confirmed that as differentiation proceeded, α-actinin expression gradually increased, and G-CSFR expression decreased (Fig. 2 b).

To clarify the effect of G-CSF on myocytes, G-CSF was administered to C2C12 cells that expressed the G-CSFR. G-CSF administration significantly increased the number of C2C12 cells in a dose-dependent manner (Fig. 2 c). BrdU incorporation analysis revealed that the increased cell number was the result of cell proliferation induced by G-CSF (Fig. 2 d). An anti–G-CSF neutralizing antibody inhibited the serum-dependent proliferation of C2C12 cells (Fig. 2 e). We also examined whether G-CSF may affect the myogenic cell differentiation.

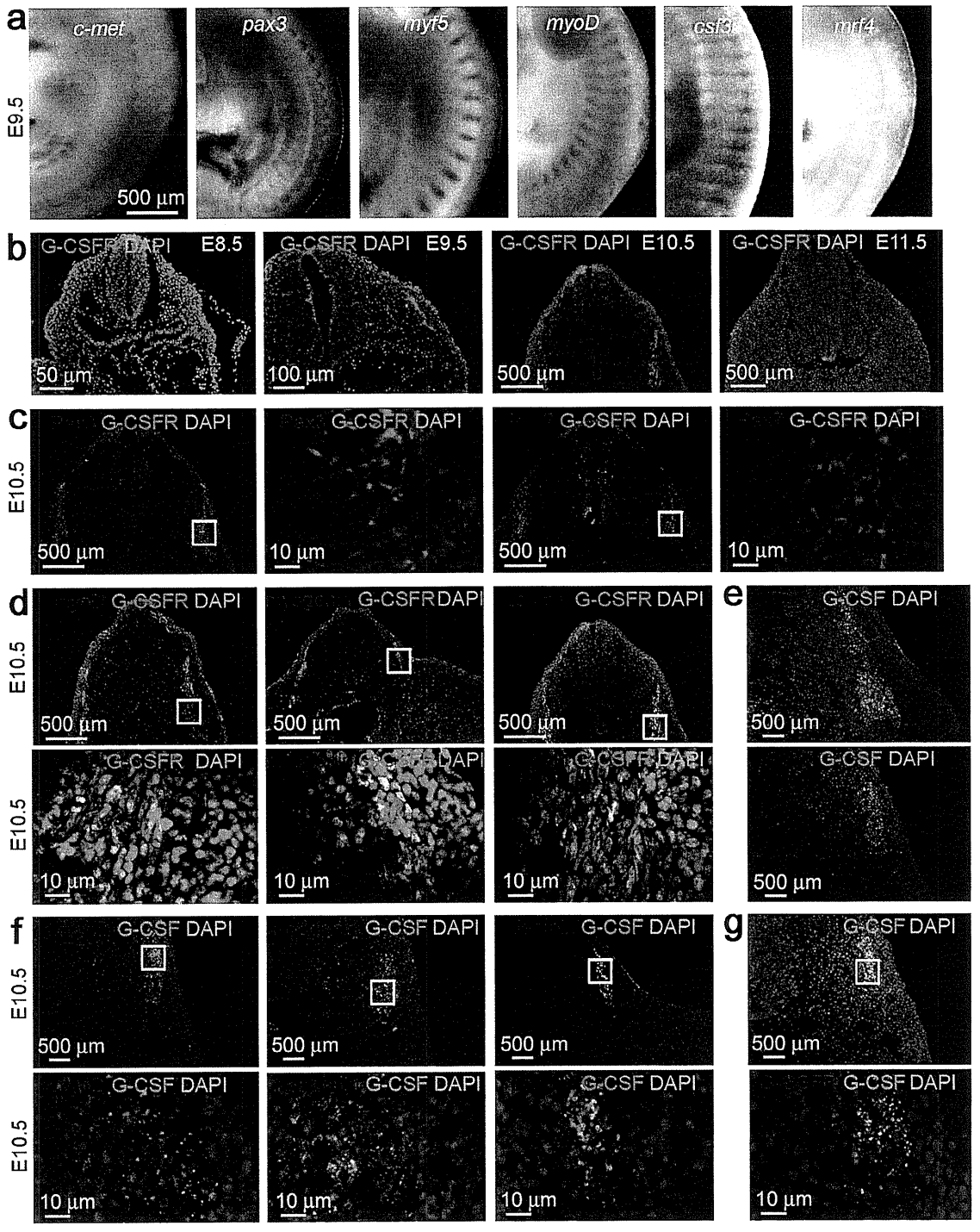

Figure 1. G-CSFR and G-CSF are expressed in developing somites after the midgestation stage. (a) Whole-mount in situ hybridization for *c-met*, *pax3*, *myoD*, *csf3r*, and *mrf4* in E9.5 embryos. The β-galactosidase staining for *myf5* nLacZ knockin mice in E9.5 embryo is also shown. (b) Immunostaining for G-CSFR and nuclei (DAPI) in E8.5, E9.5, E10.5, and E11.5 mouse embryos. (c) Triple immunofluorescence staining for Pax3, Pax7, and G-CSFR in an E10.5 embryo. DAPI indicates nuclear stain. (d) Triple immunofluorescence staining for MyoD, myogenin, desmin, G-CSFR, and nuclei (DAPI) in an E10.5 embryo. (e) Triple immunostaining for G-CSF, Pax3, Pax7, and nuclei (DAPI) in an E10.5 embryo. (f) Triple immunofluorescence staining for MyoD, myogenin, desmin, G-CSF, and nuclei (DAPI) in an E10.5 embryo. (g) Triple immunostaining for G-CSFR, G-CSF, and nuclei (DAPI) in an E10.5 embryo. (c, d, f, and g) Boxed areas are shown at higher magnification in the images to the right (c) or below (d, f, and g). Representative photographs in a are from three independent experiments with 10 embryos. Results in b–g are from five independent experiments.

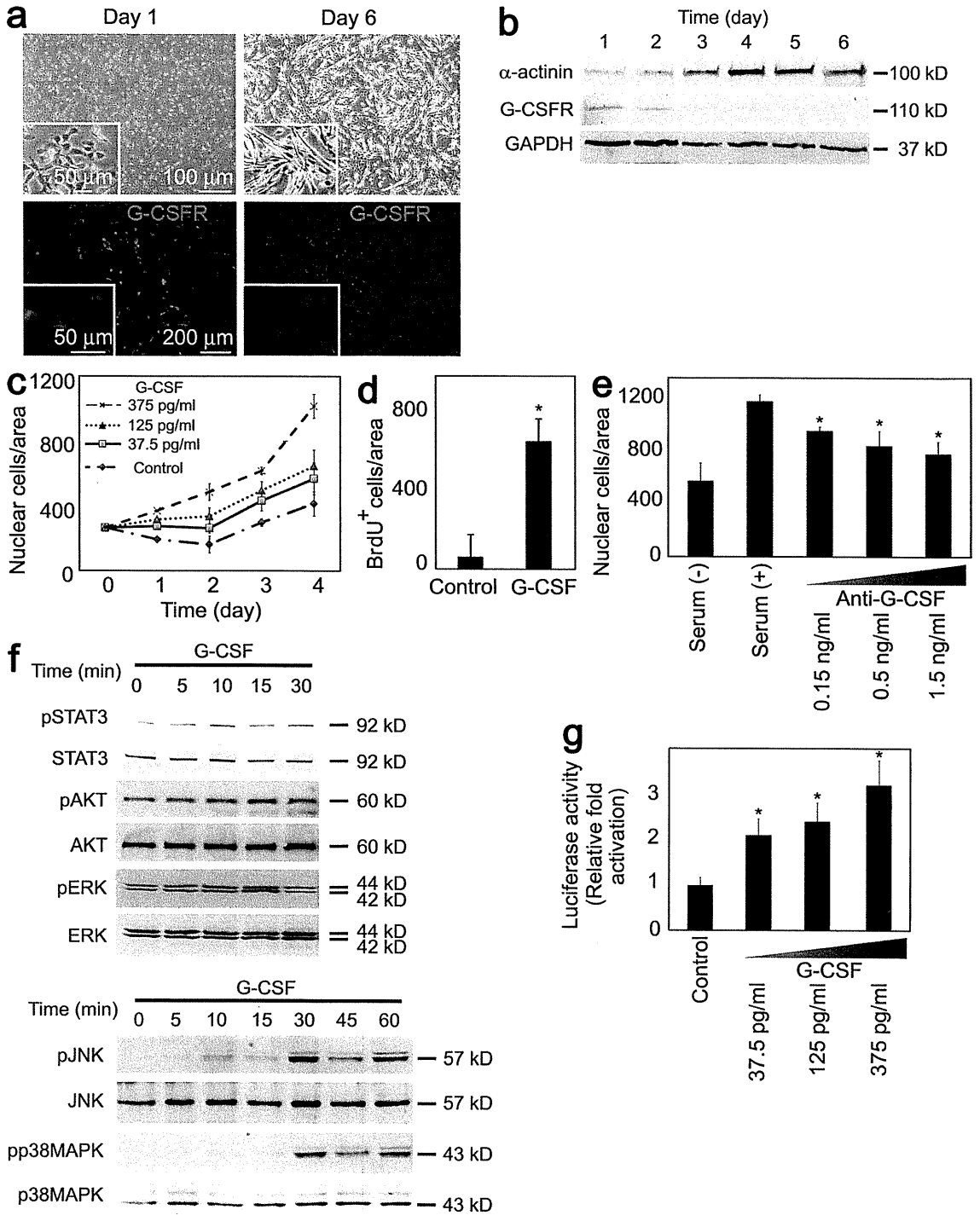

Figure 2. G-CSF increases myoblast proliferation. (a) Phase-contrast micrography (top) and immunofluorescence (bottom) imaging of G-CSFR and α-actinin in C2C12 myoblast cell line before (day 1) and during (day 6) differentiation induced by low-serum conditions. Inset images are shown at higher magnification. (b) G-CSFR and α-actinin expression was analyzed by Western blot in differentiating C2C12 cells. GAPDH was a loading control. (c) C2C12 cells were cultured with or without the indicated concentrations of G-CSF in low-serum conditions. Cells were counted at the indicated time points. (d) C2C12 cells were cultured with or without G-CSF in low-serum conditions and were pulsed with BrdU. BrdU incorporation was measured at day 3 of differentiation. (e) C2C12 cells were incubated without serum or with serum and the indicated concentrations of G-CSF neutralizing antibody. Cells were counted on day 5 of culture. (f) C2C12 cells were cultured with or without G-CSF for the indicated time points, and phosphorylated and total

G-CSF was administered during C2C12 differentiation at different time points (Fig. S1 a), and myocyte differentiated marker expression was examined. Although G-CSF significantly increases the number of myocytes, G-CSF didn't affect the myocyte differentiated marker expression (Fig. S1 b). Thus, G-CSF plays an essential role in C2C12 cell proliferation.

The binding of G-CSF to its receptor activates various signals, including extracellular regulated kinase (ERK), c-Jun N-terminal kinase (JNK), p38MAPK, AKT, and STAT, in hematopoietic cells (Avalos, 1996). We confirmed that G-CSF activated STAT3, AKT, ERK, JNK, and p38MAPK in C2C12 cells in a time-dependent manner (Fig. 2 f). Of these factors, STAT3 has been reported to contribute to the proliferation of myocyte precursor cells (Megeney et al., 1996; Serrano et al., 2008). G-CSF addition to C2C12 cell cultures increased the activity of acute phase response element (APRE) luciferase, which responds to STAT3 activation (Fig. 2 g). These results indicate that G-CSF promotes the proliferation of C2C12 myoblasts through G-CSFR.

The G-CSFR is transiently expressed in regenerating skeletal myocytes

In general, the regeneration process resembles the mechanism of physiological development. Based on the finding that G-CSFR was transiently expressed in the developing somite, we expected that regenerating skeletal muscle would express G-CSFR and examined whether it was expressed in regenerating skeletal myocytes after injury. Cardiotoxin damages the myofiber plasma membrane but leaves the basal lamina, satellite cells, and nerves intact, allowing rapid and reproducible muscle regeneration (Hosaka et al., 2002). We injected cardiotoxin directly into the femoral muscles and performed a serial histological analysis up to day 28 after injury. After cardiotoxin injection, spontaneous regeneration of the injured muscle was observed (Fig. 3 a and Fig. S2). From day 1 to 2, several inflammatory cells infiltrated the injured muscle, and the injured myotubes were absorbed. The number of satellite cells or transient-amplifying cells began to increase from day 3, and regenerating myocytes that have centrally located nuclei were clearly identified from day 5 (Yan et al., 2003; Shi and Garry, 2006; Clever et al., 2010). These cells fused and rapidly increased in diameter thereafter. The injured area was filled with the regenerated myotubes, which had centrally located nuclei and smaller diameters than the matured myotubes from day 7. On day 28, the regenerated myotubes had almost the same diameter as the noninjured myotubes, although they had centered nuclei.

Triple immunostaining for laminin, G-CSFR, and DAPI revealed the absence of G-CSFR–positive cells in the noninjured skeletal muscle (Fig. 3 b). In contrast, G-CSFR was clearly expressed in the regenerating myocytes on day 5 after cardiotoxin injection (Fig. 3 c). The G-CSFR–positive cells were larger than the infiltrated inflammatory cells, round-shaped with centrally located nuclei, and completely surrounded by laminin. Thus, these cells were identified as regenerating early myocytes that expressed G-CSFR. Serial immunofluorescence staining analyses showed that the G-CSFR–expressing cells appeared only from day 3 to 8 after injury (Fig. 3, d and e).

Muscle repair is characterized by discrete stages of regeneration. In this time period, skeletal muscle regeneration involves the activation of satellite cell or transient-amplifying cell proliferation, differentiation, and maturation (Shi and Garry, 2006). The G-CSFR–expressing day corresponds to the skeletal muscle progenitor cell proliferation day.

Exogenous G-CSF augments skeletal muscle regeneration

To determine whether external administration of G-CSF facilitates skeletal myocyte regeneration, G-CSF was injected after skeletal muscle injury. G-CSF was administered i.v. or was injected i.m. into the injured muscle on day 4 and 6, at which time point G-CSFR was strongly expressed, and skeletal muscle regeneration was observed on day 7. For higher G-CSF dosages, i.v. administration was more effective for skeletal muscle regeneration than PBS administration. For lower G-CSF dosages, i.m. administration was more effective than i.v. (Fig. 4 a). The number of regenerating myocytes was significantly increased by G-CSF administration, and G-CSF administered i.m. significantly augmented skeletal muscle regeneration (Fig. 4 b). G-CSF administration also significantly increased the diameter of the regenerated muscle. The diameter of the rectus femoris was increased to a greater extent by G-CSF administered i.m. than i.v. (Fig. 4 c). Functional recovery was assessed by measuring handgrip strength after cardiotoxin injection into forearm muscles. G-CSF treatment significantly improved functional recovery on 5 and 7 d after skeletal muscle injury (Fig. 4 d).

To investigate whether innate G-CSF signaling is necessary for skeletal myocyte regeneration, an anti–G-CSF neutralizing antibody was administered after injury. This antibody reduced spontaneous skeletal myocyte regeneration in a dose-dependent manner (Fig. 4 e). The number of regenerating myocytes was drastically deceased by treatment with the anti–G-CSF antibody (Fig. 4 f). The diameter of the injured muscle was also significantly decreased by treatment with the anti–G-CSF antibody (Fig. 4 g). Individual skeletal myocyte areas in G-CSF treatment and anti–G-CSF neutralizing antibody addition were measured at day 7 after injury. At day 7, there was a substantial amount of regenerating myocytes, which were small compared with uninjured myocytes. So, the mean of

proteins were measured by Western blot. p, phospho. (g) C2C12 cells were transfected with a STAT3-responsive APRE luciferase reporter construct and were cultured with or without the indicated concentrations of G-CSF. Luciferase activity (relative to control) was measured on day 2 of culture. (c–e and g) Error bars present mean ± SD (*, $P < 0.05$). Micrographs in a are representative of five independent experiments. Results in b and f are from three independent experiments. Results in c–e and g are from five independent experiments.

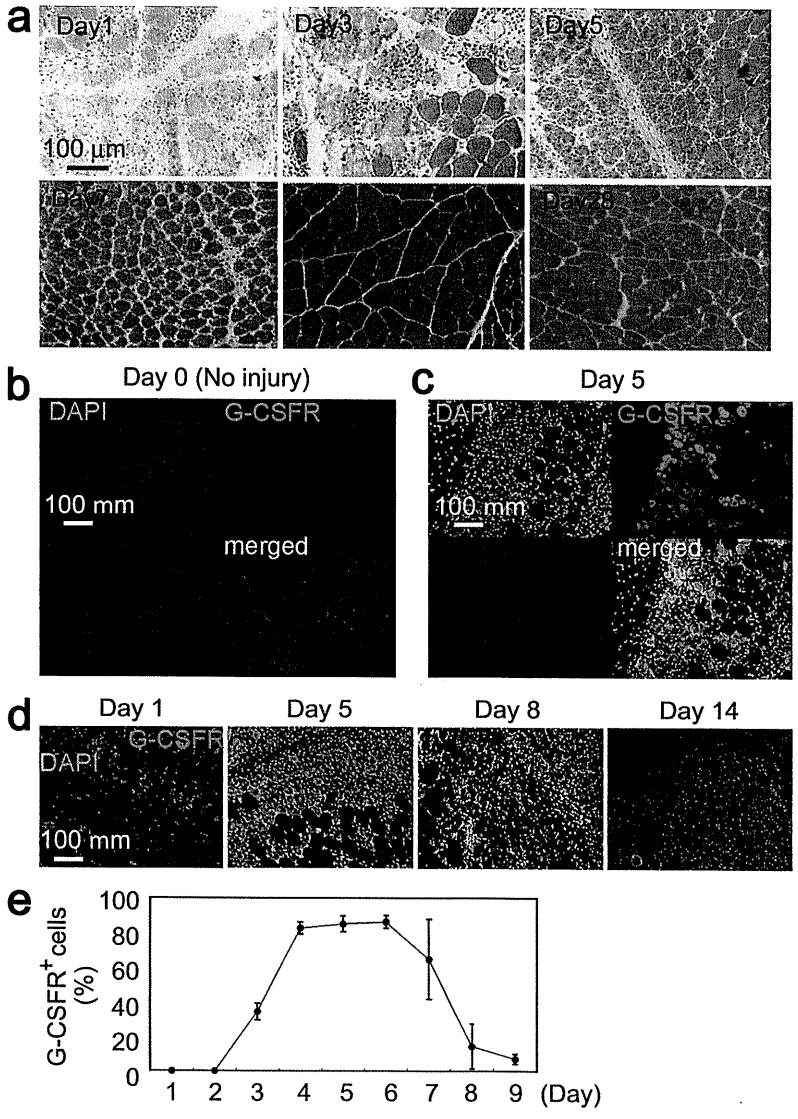

Figure 3. The G-CSFR is expressed in adult regenerating skeletal myocytes. (a) Histological analysis of cardiotoxin-injured skeletal muscle. Hematoxylin and eosin staining of the rectus femoris. (b and c) Triple immunostaining of noninjured (b; day 0) and injured (c; day 5) skeletal muscles for the detection of G-CSFR, laminin, and nuclei (DAPI). (d) Time course of G-CSFR expression in regenerating skeletal myocytes. Immunofluorescently stained injured skeletal muscles on days 1, 5, 8, and 14 are shown. (e) Percentages of G-CSFR–positive cells. The percentages of G-CSFR–positive regenerating skeletal muscle cells were assessed on days 1–9 after injury. Error bars present mean ± SD. Representative photomicrographs in a are from three independent experiments. Results in b–e are from five independent experiments.

individual skeletal myocyte areas is inversely correlated with regeneration in G-CSF treatment and anti–G-CSF neutralizing antibody administration (Fig. 4 h). However, at day 14, regenerated myocytes grew up to uninjured muscle, and there were no significant differences among those groups (unpublished data). These results indicate that exogenous G-CSF augments skeletal myocyte regeneration and that physiological G-CSF signaling plays an essential role in innate skeletal myocyte regeneration.

The *csf3r*$^{-/-}$ mouse shows impaired skeletal muscle development and regeneration

To clarify the roles of G-CSF and G-CSFR signaling in skeletal myocytes, G-CSFR–knockout (*csf3r*$^{-/-}$) mice were used. To date, *csf3r*$^{-/-}$ mice have been used mainly in hematologic studies. The number of delivered *csf3r*$^{-/-}$ mice was approximately half as many as that of wild-type (*csf3r*$^{+/+}$) mice. Normally, delivered *csf3r*$^{-/-}$ mice showed no significant differences in appearance. When fully grown, the body size of the *csf3r*$^{-/-}$ mouse was slightly but significantly smaller than that of the *csf3r*$^{+/+}$ mouse. The initial histological analysis of the skeletal muscle of the *csf3r*$^{-/-}$ mouse revealed no significant difference compared with that of the *csf3r*$^{+/+}$ mouse (Fig. 5 a). However, in the sections of skeletal muscles, the myocytes were slightly but significantly larger in the *csf3r*$^{-/-}$ mice than in the *csf3r*$^{+/+}$ mice (Fig. 5 b). Moreover, the diameter of the rectus femoris was significantly smaller in the *csf3r*$^{-/-}$ mouse than in the wild-type mouse (Fig. 5 c). Although skeletal myocyte proliferation is correlated with hypertrophy in some situations, the molecular pathway of skeletal myocyte proliferation is an independent event of skeletal muscle hypertrophy (Rantanen et al., 1995; Adams et al., 1999; Armand et al., 2005; Philippou et al., 2007). And more, skeletal muscle hypertrophy is an adaptation process for physiological requirements (Sakuma et al., 2000; Solomon and Bouloux, 2006). These findings suggest that in the *csf3r*$^{-/-}$ mouse, skeletal muscle proliferation is reduced during development, and, as a consequence, the skeletal myocytes are adaptively hypertrophic.

To investigate whether innate G-CSFR is necessary for skeletal myocyte regeneration, *csf3r*$^{-/-}$ mice were subjected to cardiotoxin-induced skeletal muscle injury. The *csf3r*$^{-/-}$ mice showed deterioration of skeletal muscle regeneration on day 7 and 14 after injury in the rectus femoris muscles (Fig. 5 d). The number of regenerating myocytes in the regenerating skeletal muscle was significantly decreased in the *csf3r*$^{-/-}$ mice (Fig. 5 e), which suggests the G-CSFR is essential for skeletal muscle regeneration. To confirm that the observed effect of G-CSF occurred through the G-CSFR, we administrated

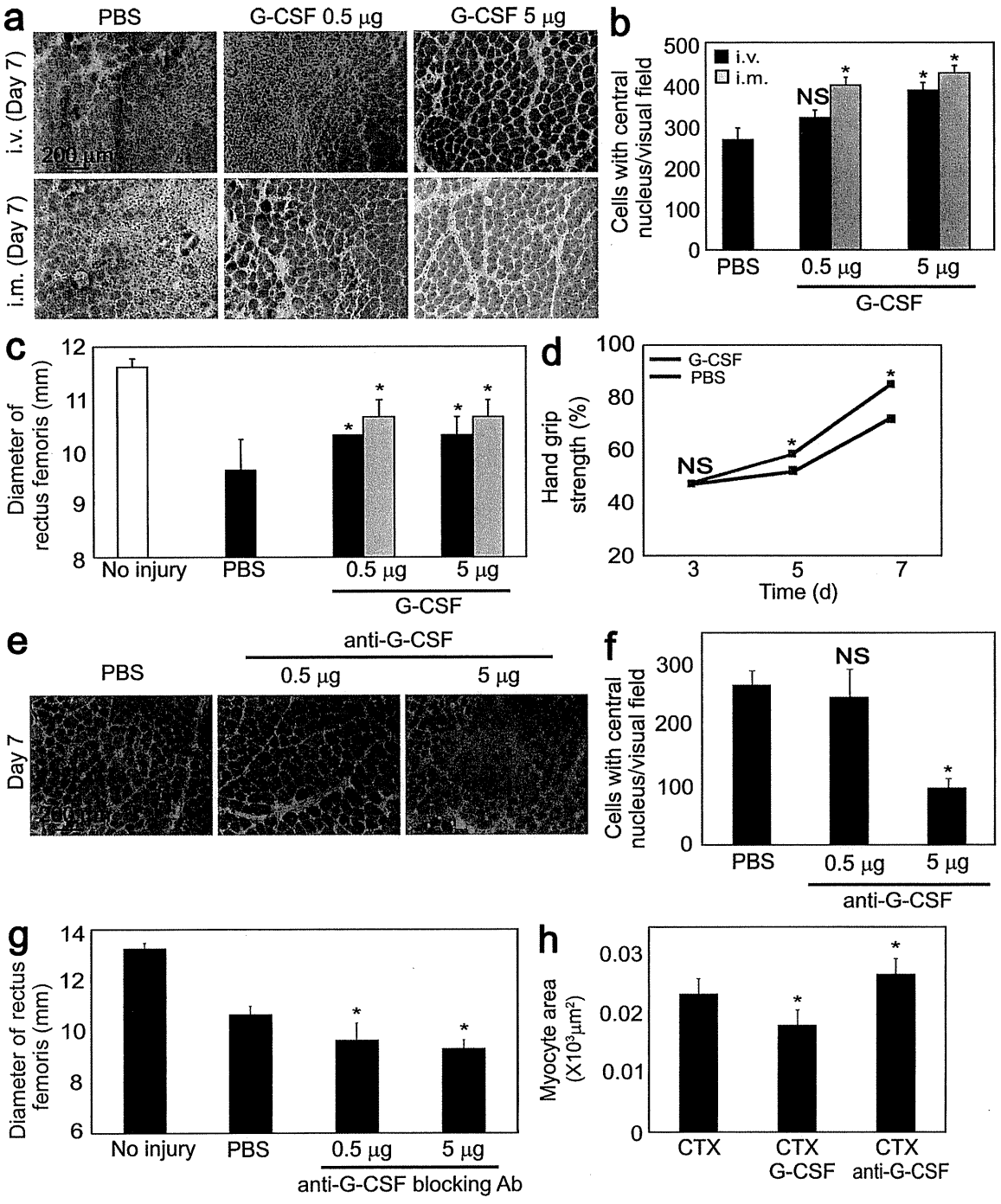

Figure 4. Both intrinsic and extrinsic G-CSF augment skeletal muscle regeneration. (a) Effect of i.v. or i.m. administration of G-CSF on cardiotoxin-induced skeletal muscle injury. Hematoxylin and eosin staining of injured rectus femoris 7 d after cardiotoxin injection. (b) Numbers of regenerating myocytes that have centrally located nuclei. 20 visual fields per individual mice were observed in the rectus femoris at 7 d after cardiotoxin injection. (c) Diameter of the regenerated rectus femoris at 7 d after cardiotoxin injection. (d) Handgrip strength on day 3–7 after cardiotoxin injury. (e) Role of the intrinsic G-CSF signal in skeletal muscle regeneration. Hematoxylin and eosin staining of an injured rectus femoris on day 7 is shown. (f) Numbers of regenerating myocytes that have centrally located nuclei. 20 visual fields per individual mice were observed in the rectus femoris at 7 d after cardiotoxin injection. (g) The diameter of the injured rectus femoris is shown with or without the anti-G-CSF neutralizing antibody (Ab) at 7 d after cardiotoxin injection. (h) Quantitative analysis of the areas of the skeletal myocyte sections. CTX, cardiotoxin. (b–d and f–h) Error bars present mean ± SD (*, $P < 0.05$). Results in a–h are from eight independent experiments.

G-CSF to the *csf3r*$^{-/-}$ mice. If G-CSF functions through other receptors, the addition of G-CSF should still improve the skeletal muscle regeneration of *csf3r*$^{-/-}$ mice. Exogenous G-CSF administration didn't improve skeletal muscle regeneration (Fig. 5 f). The numbers of regenerating myocytes in the regenerating skeletal muscles were measured. G-CSF administration significantly increased the numbers of regenerating myocytes in the *csf3r*$^{+/+}$ mice but not in the *csf3r*$^{-/-}$ mice (Fig. 5 g). Functional recovery was assessed by measuring handgrip strength after cardiotoxin injection into forearm muscles.

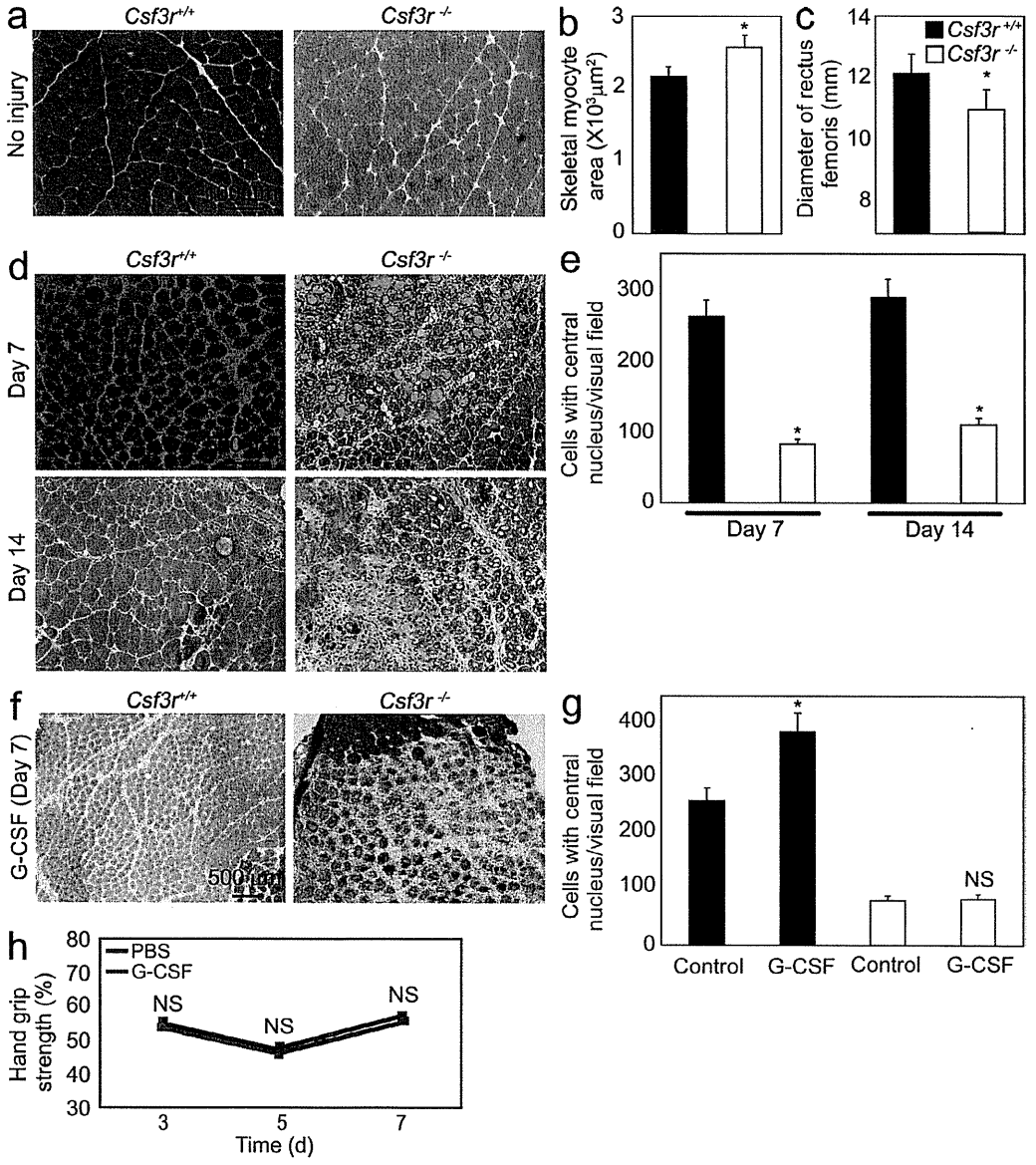

Figure 5. The *csf3r*$^{-/-}$ mouse shows impaired skeletal muscle development and regeneration. (a) Hematoxylin and eosin staining of the rectus femoris of a wild-type mouse and a *csf3r*$^{-/-}$ mouse. (b) Quantitative analysis of the areas of the skeletal myocyte sections in the wild-type and *csf3r*$^{-/-}$ mice. (c) The diameter of the rectus femoris is shown. (d) Hematoxylin and eosin staining of the cardiotoxin-injured skeletal muscles of the wild-type and *csf3r*$^{-/-}$ mice at 7 and 14 d after injury. (e) Numbers of regenerating myocytes that have centrally located nuclei on days 7 and 14 after injury in the regenerating skeletal muscles of the wild-type and *csf3r*$^{-/-}$ mice. 20 visual fields per individual mice were observed in the rectus femoris. (f) Effects of extrinsic G-CSF administration on cardiotoxin-induced muscle injury in the wild-type and *csf3r*$^{-/-}$ mice. Hematoxylin and eosin staining of injured skeletal muscle on day 7 after cardiotoxin injection is shown. (g) Effect of extrinsic G-CSF administration on cardiotoxin-induced skeletal myocyte injury, as assessed by the numbers of regenerating myocytes. 20 visual fields per individual mice were observed in the rectus femoris at 14 d after cardiotoxin injection. (b, c, e, and g) Error bars present mean ± SD (*, $P < 0.05$). (h) Handgrip strengths of cardiotoxin-injected *csf3r*$^{-/-}$ mice with or without G-CSF treatment. Results in a–h are from eight independent experiments.

G-CSF administration didn't confer functional recovery on day 5 or 7 after injury (Fig. 5 h). To elucidate precise myoblast function, we also examined the proliferation ability of *csf3r*$^{-/-}$ myoblasts in vitro. The *csf3r*$^{-/-}$ myoblasts showed significant decreased proliferation ability (Fig. S1 c). However, the expression of myocyte differentiation marker was not altered, which indicates that myocyte differentiation ability was not impaired in *csf3r*$^{-/-}$ myoblasts (Fig. S1 d).

G-CSFR–expressing BM cells do not recover skeletal muscle regeneration in the *csf3r*$^{-/-}$ mouse

To clarify the involvement of hematopoietic cells or BM cells in the impairment of skeletal muscle regeneration, we transplanted the BM cells from *csf3r*$^{+/+}$ mice, which constitutively expressed GFP, to the *csf3r*$^{-/-}$ mice (Fig. 6 a) 60 d before cardiotoxin-induced injury. In all the mice, the BM cells stably engrafted, and chimerism was >80%, as assessed by FACS (Fig. S3 a). After cardiotoxin injection into forearm muscles, the *csf3r*$^{-/-}$ mice that were transplanted with BM cells from *csf3r*$^{+/+}$ mice didn't show any improvement in gross morphology, the number of central cells, and handgrip strength after G-CSF treatment (Fig. 6, b–d). Moreover, the diameter of rectus femoris in these mice wasn't improved by G-CSF treatment after cardiotoxin injection into the rectus femoris muscles (Fig. 6 e). These mice showed no significant improvement in the regeneration by G-CSF treatment, and myocyte area was not altered by G-CSF treatment either (Fig. S3 b).

Next, we performed the BM transplantation experiment in reverse; the BM cells from *csf3r*$^{-/-}$ mice were transplanted into *csf3r*$^{+/+}$ mice. In these mice, skeletal muscle injury was generated, and regeneration was induced with G-CSF (Fig. 6 f). G-CSF treatment markedly improved gross morphology, the number of central cells, and handgrip strength after cardiotoxin injection into forearm muscles (Fig. 6, g–i) and increased the diameter of the rectus femoris after cardiotoxin injection into the rectus femoris muscles (Fig. 6 j). These mice showed more regeneration, and mean myocyte area was decreased by G-CSF treatment (Fig. S3 c). These results indicate that G-CSF promotion of skeletal muscle regeneration is a direct effect on skeletal muscle and isn't mediated by BM cells.

DISCUSSION

This study demonstrates that G-CSF and G-CSFR play pivotal roles in skeletal myocyte development and regeneration. Interestingly, this mechanism about G-CSF and G-CSFR is conserved between embryonic skeletal myocyte development and adult skeletal myocyte regeneration. G-CSFR is transiently but strongly expressed in myoblasts during development. The total mass of skeletal muscle is lower in *csf3r*$^{-/-}$ mice than in *csf3r*$^{+/+}$ mice, which means that G-CSF and G-CSFR signaling are essential for proper skeletal muscle development. G-CSFR is also expressed in the regenerating adult myocyte. G-CSF stimulates these G-CSFR–expressing myoblasts and promotes skeletal muscle regeneration after injury. The *csf3r*$^{-/-}$ mice showed drastic impairment of skeletal muscle regeneration, which suggests that G-CSF is critical for skeletal muscle regeneration.

During development, early muscle progenitor cells are characterized by Pax3 and Pax7 expression. Pax3 and Pax7 cooperatively specify the muscle progenitor pool because in mice deficient for both Pax3 and Pax7, all muscle progenitor cells are absent (Kassar-Duchossoy et al., 2005; Relaix et al., 2005). Once specified, muscle progenitor cells either proliferate or exit the cell cycle to undergo terminal differentiation. The latter process requires the activation of MRFs (Sabourin and Rudnicki, 2000). G-CSFR was expressed in cells that expressed MRFs but not in early muscle progenitor cells. Therefore, we speculate that rather than inducing early progenitor cells to increase the skeletal muscle stem cell pool, G-CSF causes late progenitor cells to adopt muscle mass requirement. In adult skeletal muscle, myogenic progenitor cells, which are characterized by the expression of MyoD, Myf5, or MRF4, and myoblasts, which are characterized by MyoD and Myf5 expression, are known as transient-amplifying cells (Weintraub, 1993; Shi and Garry, 2006; Kuang and Rudnicki, 2008; Biressi and Rando, 2010). We found that in the adult stage, G-CSFR was expressed in myoblasts, and G-CSF increased myocyte proliferation.

G-CSF is a hematopoietic cytokine that recruits hematopoietic cells (Cottler-Fox et al., 2003). The contribution of BM cells to muscle regeneration has been documented (Ferrari et al., 1998; Gussoni et al., 1999; LaBarge and Blau, 2002). To exclude the possibility that hematopoietic cells and BM mesenchymal stem cells affect skeletal muscle regeneration in response to G-CSF, we transferred wild-type BM cells to *csf3r*$^{-/-}$ mice. In these mice, the skeletal myocytes didn't express G-CSFR, whereas the BM cells expressed G-CSFR. If BM cells contributed to skeletal muscle regeneration, these mice would show normal or improved regeneration abilities. However, they didn't show skeletal muscle regeneration in response to G-CSF. This finding is consistent with a report that stromal progenitor cells are mobilized by vascular endothelial growth factor but not by G-CSF (Pitchford et al., 2009). We assume that the contribution of BM cells to G-CSF–mediated skeletal muscle regeneration is negligible.

Skeletal muscle regeneration is a complex process that remains to be fully understood. After muscle injury, disruption of the myofiber plasma membrane initiates an influx of extracellular calcium, leading to calcium-dependent proteolysis, which results in necrosis and degeneration of the myofibers. Several signals released from the degenerating myocytes attract and activate inflammatory cells, which secrete cytokines. Neutrophils are the first inflammatory cells to reach the injured myofibers, followed by macrophages, which phagocyte the degenerating muscle fibers (Chargé and Rudnicki, 2004). Satellite cells and macrophages interact to amplify chemotaxis and enhance inflammation. Monocytes and macrophages may support satellite cell survival by cell–cell contacts and the release of soluble factors (Chazaud et al., 2003). In addition, monocyte and macrophage infiltration leads to increased satellite cell proliferation and differentiation (Lescaudron et al., 1999).

Based on our results, we speculate that macrophages are not only important for the resolution of necrosis but also involved in the induction of muscle regeneration. These leukocytes secrete G-CSF in the presence of appropriate stimuli (Hareng and Hartung, 2002). Although previous studies showed that G-CSF seems to have some positive effects on skeletal muscle regeneration, it's not clear how G-CSF affects skeletal muscle regeneration, and especially the involvement

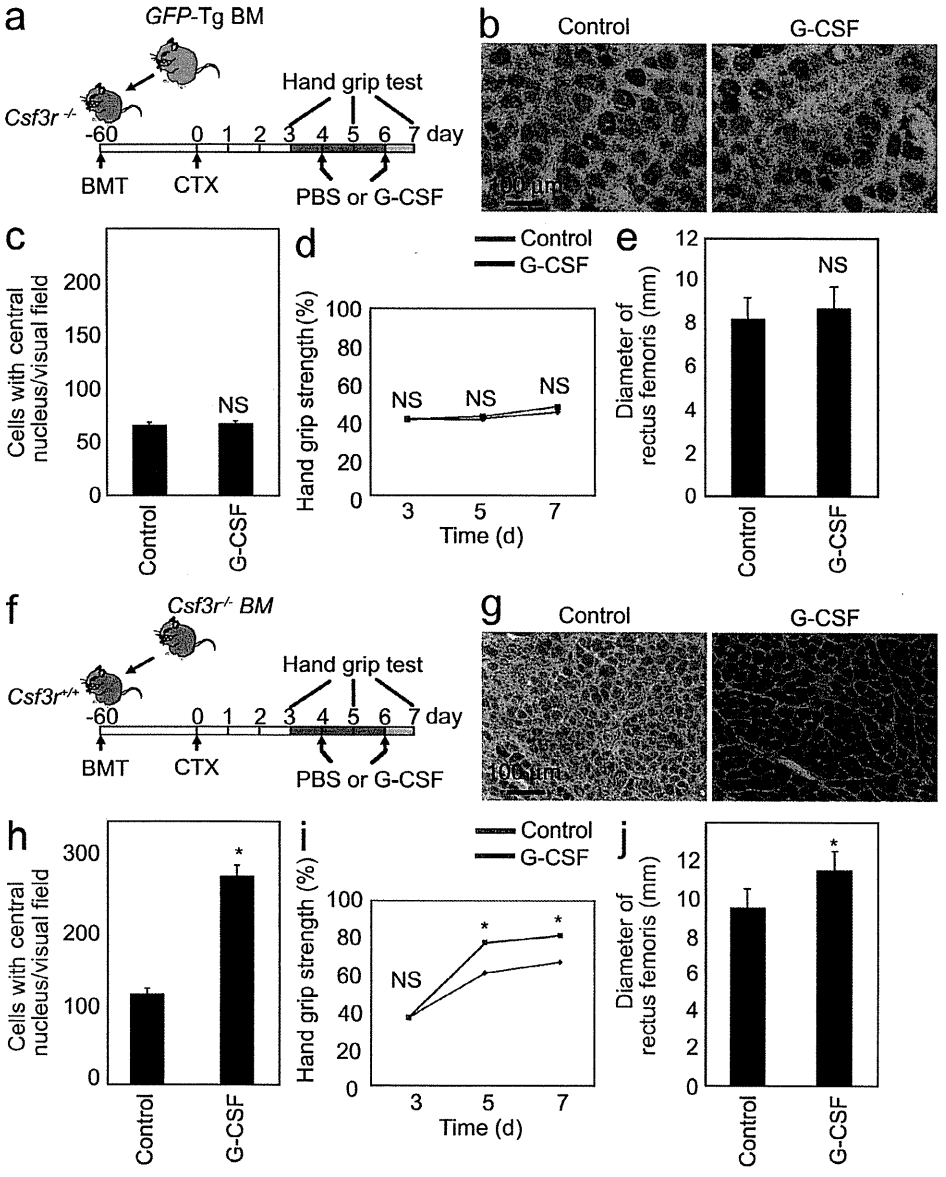

Figure 6. Effect of transplanted G-CSFR–expressing BM cells on skeletal muscle regeneration. (a) Experimental model of BM transplantation 1. BM cells were isolated from GFP-transgenic (Tg) mice and transplanted into the *csf3r*$^{-/-}$ mice. Cardiotoxin was injected into the rectus femoris, and G-CSF was administered on days 4 and 6. (b–e) Effects of G-CSF on skeletal muscle regeneration of *csf3r*$^{-/-}$ mice subjected to cardiotoxin-induced skeletal myocyte injury and transplanted with wild-type BM (from GFP-transgenic mice). (b) Hematoxylin and eosin staining of the cardiotoxin-injured skeletal muscles at 7 d after injury. (c) Effect of extrinsic G-CSF administration on cardiotoxin-induced skeletal myocyte injury, as assessed by the numbers of regenerating myocytes. 20 visual fields per individual mice were observed in the rectus femoris at 14 d after cardiotoxin injection. (d and e) Effects of G-CSF on the handgrip strength (d) and rectus femoris diameter at 14 d (e) are negligible. (f) Experimental model of BM transplantation 2. BM cells were isolated from *csf3r*$^{-/-}$ mice and transplanted into the wild-type (*csf3r*$^{+/+}$) mice. (g) Hematoxylin and eosin staining of the cardiotoxin-injured skeletal muscles at 7 d after injury. (h) Effect of extrinsic G-CSF administration on cardiotoxin-induced skeletal myocyte injury, as assessed by the numbers of regenerating myocytes. 20 visual fields per individual mice were observed in the rectus femoris at 14 d after cardiotoxin injection. (i and j) Effects of G-CSF on the handgrip strength (i) and rectus femoris diameter at 14 d (j). (c, e, and h–j) Error bars present mean ± SD (*, $P < 0.05$). Results in b–e and g–j are from eight independent experiments.